Chapter 2
Catalytic Processes

Abstract The chapter begins with a brief analysis of the advantages and disadvantages of fluidized-bed reactors compared with alternatives such as fixed beds for solid-catalysed gas-phase processes coupled with some general points about reactor operation. The points made are emphasised in the descriptions that follow of the most prominent technologies currently employing gas-solid catalytic reactions. Olefin polymerization is traced from its introduction in the 1960's to modern-day variants employing condensing-mode operation. Operational problems associated with electrostatic charging of the fluidized polymer particles are discussed. Processes for the oxidation of n-butane to maleic anhydride are presented, particular attention being paid to the DuPont circulating fluidized-bed process which although ultimately ending in failure demonstrated important aspects of plant design and operation. Well-established processes for the ammoxidation of propylene to acrylonitrile are discussed the emphasis being on that developed by Sohio. Processes for the production of vinyl chloride monomer and vinyl acetate monomer are described briefly. A section on gas-to-liquid technologies describes the classic Synthol process as well as more recent developments converting synthesis gas to methanol and thence to gasoline and light olefins. The chapter concludes with a consideration of fluidized catalytic cracking, arguably the most important catalytic reaction in all industry. In each case the emphasis is on process chemistry, catalyst formulation, reactor configuration and operation and reactor/process modelling.

2.1 Introduction

Processes based on the use of heterogeneous catalysts lie at the heart of the chemical and allied industries and of the many types of reactor employed in these processes the fluidized bed offers a number of advantages over alternative designs. In beds operated at high gas velocities in the bubbling and turbulent regimes referred to earlier bed particles are in constant motion and as a result are well mixed. Thus any hot spots that may arise in an exothermic reaction are rapidly quenched and the bed operates essentially isothermally. A further consequence of

J.G. Yates and P. Lettieri, *Fluidized-Bed Reactors: Processes and Operating Conditions*, Particle Technology Series 26,
DOI 10.1007/978-3-319-39593-7_2

good solids mixing is that heat transfer between bed material and immersed surfaces is highly efficient so that with appropriate design of heat exchangers beds may be operated within closely controlled temperature limits. Another advantage is the ability to introduce multiple feeds directly into the bed without the necessity of pre-mixing, something difficult to achieve with a fixed-bed reactor. Further the liquid-like properties of fluidized solids enable them to be transferred smoothly from one reactor to another for catalyst regeneration and reheating as in the FCC process. Once the catalyst particles are fluidized the pressure drop across the reactor, unlike for fixed-bed reactors, remains more or less constant with increasing gas velocity so for high gas throughputs and equivalent bed heights pressure drops through fluidized beds are lower than through fixed beds leading to lower compression costs in the former case. Another advantage is that the use of small particles ensures effectiveness factors are close to unity (Jiang et al. 2003).

There are however a number of disadvantages of fluid-bed operation such as gas back-mixing leading to the formation of unwanted side products, particle attrition leading to loss of catalyst through cyclones, and erosion of bed internals by the sand-blasting effect of the moving particles. Because of the frequently complex hydrodynamics of fluidized beds scale-up can be challenging. These and other considerations will be explored in the context of the individual processes described below.

The majority of fluidized-bed reactors used in catalytic processes are operated at high gas velocities in the turbulent, circulating or fast regimes (Fig. 1.1).

The reactors have several features in common—cylindrical vessels of relatively high aspect ratio fitted at their lower end with a gas distributor at their upper end with one or more cyclone separators and often packed in between with heat-transfer tubes or coils. The distributor or grid spans the cross-section of the bed at its base above the windbox or plenum chamber into which the fluidizing gas is admitted. Distributors should be designed so as to maintain the bed solids in uniform motion and prevent the formation of defluidized zones, operate for long periods without plugging, minimise attrition of bed particles and minimise the leakage of particles into the plenum. A number of different designs have been used and classified according to the direction of gas entry: upward, laterally or downward (Karri and Werther 2003) through bubble caps, nozzles, spargers, conical grids and pierced sheets. The entry points are frequently arranged on a square or triangular pitch, open holes often being fitted with shrouds, short lengths of pipe centred over the holes, to help reduce particle attrition. In order to maintain a constant and uniform fluidization in the bed it is necessary to maintain a sufficiently high pressure drop, Δp_D, across the grid. This is normally considered in relation to the pressure drop across the bed as a whole, Δp_B, the value depending on the direction of gas entry. Thus Karrie and Werther (2003) propose:

$$\Delta p_D = 0.3 \Delta p_B$$

for upward and laterally directed flow, and:

$$\Delta p_D = 0.1 \Delta p_B$$

for downward flow and furthermore that the pressure drop across a large-scale grid should never be less than 2500 Pa.

The function of the cyclone at the exit of the bed is to separate gases from solids so as to minimise particulate emissions and return catalyst material to the bed. They act by causing a centrifugal force to be acted on the particles forcing them to the wall of the vessel where they lose momentum and spiral downwards via a dipleg and flapper valve back to the bed. The separated gas flows upwards and out of the unit.

Cyclones have the advantages of having no moving parts, being inexpensive to construct, having low pressure drops and low maintenance costs. To increase solids collection efficiencies they are sometimes operated in series, two-stage cyclones in fluidized catalytic cracking regenerators, for example, having efficiencies of over 99.999 % (Knowlton 2003).

Other detailed aspects of reactor design and operation will be discussed in the context of the individual processes that follows.

2.2 Some Individual Processes

2.2.1 Olefin Polymerization

2.2.1.1 Process Background

As mentioned above (Sect. 1.2.3.1) the Union Carbide company introduced the first fluid-bed process for the polymerization of olefins in 1968 and since then a number of other companies, notably Sumitomo, Mitsui, BASF, ExxonMobil and BP, have commercialized similar technology. A schematic of the Unipol process is shown in Fig. 2.1.

The reactant gases, ethylene and co-monomers such as butene, are fed along with very small silica-supported catalyst particles into the base of the reactor at three to six times the minimum fluidization velocity of the larger bed particles (Kunii and Levenspiel 1991). The reactor contains preformed polyethylene particles maintained at 40–120 °C and 10–40 kPa pressure. As the catalytic reaction proceeds the polymer particles grow up to 5000 μm in size the product being withdrawn from the reactor so as to keep the bed at more or less constant volume. They are removed at a point above and close to the distributor through sequential operation of a pair of timed valves and separated from unreacted gases which are then recycled. Temperature control is crucial to successful operation since the

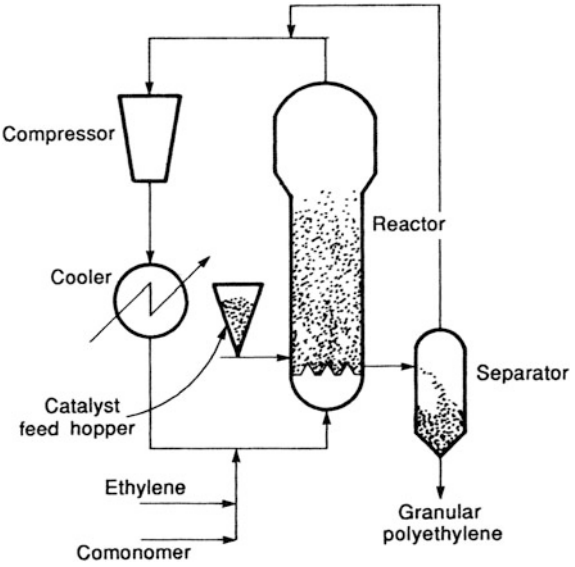

Fig. 2.1 The Unipol process for the production of polyethylene (Kunii and Levenspiel 1991)

reaction is highly exothermic and the bed operates close to the melting point of the polymer. Indeed the production rate is limited by the maximum rate at which heat can be removed from the reactor. As a result per-pass conversion is kept low at around 1–2 %, unreacted gases being recycled and cooled before being readmitted to the reactor. Because of the potential build-up of polymer deposits internal cooling coils cannot be used so early units such as that shown employed external heat exchangers. The Unipol process and similar variants have been comprehensively reviewed by Xie et al. (1994). Modern designs operate in the condensing mode where a proportion of the recycle gas is cooled to below its dew point to form liquid before its readmission to the reactor; the latent heat of evaporation of the liquid is then used to aid temperature control. Operation in the condensing mode has enabled newer plants to increase capacity by up to 200 % (Jazayeri 2003) i.e. of the order of 200,000 tonnes per year.

The beds operate in the turbulent flow regime. Bed particles have the physical properties of Group B materials (d_p = 300–5000 μm, ρ_p = 550–850 kg/m^3) but owing to the high pressure of operation they show Group A behaviour i.e. smooth fluidization and extensive emulsion-phase expansion (Burdett et al. 2001).

The process may be used to produce a wide range of products including homo- and copolymers of ethylene and propylene or copolymers containing one or more C_3 to C_8 alpha-olefins. Linear low density polyethylene (LLDPE) is made from copolymers of ethylene, butene, 4-methylpentene-1 or hexene while high density polyethylene (HDPE) results from homopolymerization of ethylene or copolymerization with butene, pentene, hexene, 4-methylpentene-1 or octene.

2.2.1.2 Condensing-Mode Operation

In a version of the process developed by BP (Chinh et al. 1998)the main body of the reactor is a cylindrical vessel with a gas distributor at its lower end, the distributor being a flat or dished plate perforated by equally distributed holes some 5 mm in diameter; distributor grids are often designed with relatively large holes without nozzles (Yamamoto et al. 1998). In the upper part of the reactor with an expanded cross-sectional area the gas velocity is decreased enabling some entrained particles to be returned to the bed below. The gases exiting the reactor pass to a cyclone where fines are separated, the gas then passing to a heat exchanger and a compressor; a second heat exchanger removes the heat of compression. The two exchangers are operated so as to cause a proportion of the recycle gas to be condensed, the gas-liquid recycle stream then passing to a separator where the liquid condensate is removed and pumped back into the reactor. The separated gas is recycled to the bed along with the amount of monomer/comonomer required to replace that consumed during the polymerization. In the BP process the liquid condensate is injected into the fluidized bed through a multi-orifice nozzle located at a distance above the gas distributor where the bed temperature has reached that required for the polymerization. The liquid condensate may be a condensable monomer such as butene, hexene or octene or an inert condensable liquid such as butane, pentane or hexane. The mass ratio of liquid to total gas injected can cover a wide range e.g. 6:100 to 25:100 depending on the activity of the catalyst and the required production rate. Hydrogen is added to the recycle stream to act as a chain-transfer agent in the polymerization reaction to control the molecular weight of the product.

2.2.1.3 Catalysts

Heterogeneous catalysts for the polymerization of alpha-olefins were introduced by Ziegler and Natta in the 1950's. They were based on transition metal halides such as $TiCl_4$ in combination with an organo-aluminium compound such as aluminium tri-ethyl. Depending on the exact formulation of the catalyst and the processing conditions the polymer products were found to have varying stereospecific structures at the resulting chiral centres. Thus polypropylene could have one of three so-called tacticities: isotactic where the chiral centres were all similarly orientated i.e. all either *d* or *l*, syndiotactic where they were alternately *d* and *l*, or atactic where the chiral centres were randomly distributed. Similar structures were found to result from using chromium-based coordination compounds developed around the same time by the Phillips company.

In recent years a new class of polymerization catalysts has been introduced constituting a major advance on the earlier materials. These are the metallocenes one example of which is dicyclopentadieneylzirconium dichloride $(C_5H_5)_2ZrCl_2$ activated in a similar manner to Ziegler-Natta catalysts by an aluminium compound methylaluminoxane (MAO) $Al_4O_3(CH_3)_6$. The metallocenes are soluble in

hydrocarbons and with easily variable structures enable the properties of the resulting polymers to be accurately predicted with controllable molecular weight distributions and tacticities. In addition they are 10–100 times more active than Ziegler-Natta systems, a combination of zirconocene and MAO allowing the polymerization of 100 tonnes of ethylene per gram of zirconium (Kaminsky 1998); they are so active that there is no requirement to separate them from the polymer product at the end of the process.

To be used in fluidized-bed polymerization reactors the catalysts must be impregnated into solid supports such as particles of silica, alumina or preformed polyolefin although silica is the preferred support. The amounts of metallocene and activator are in the range 0.01–0.5 and 0.5–20 mmol per gram of carrier particles respectively (Yamamoto et al. 1998). The porous silica-based catalyst particles are normally produced by spray drying.

During reaction polymer growth occurs within catalyst pores until hydraulic pressure fractures the particle; an outer polymer shell then develops and the particles continue to fragment exposing additional active sites (Burdett et al. 2001). The process has been described in detail in Xie et al. (1994).

2.2.1.4 Electrostatic Effects

The polymer particles produced in the fluidized-bed polymerization process have dielectric properties and as a result of their frequent frictional contacts with other bed particles and with the walls of the reactor they generate electrostatic charges. This is known as "triboelectrification" and is frequently observed in fluidized beds of dielectric or refractory particles (Boland and Geldart 1971). In the case of olefin-polymerization reactors electrostatic forces can cause particles to adhere to the reactor walls especially on the sloped region of the upper disengaging zone where they overheat and fuse together due to the exothermic heat of reaction. Particles behaving in this way are referred to as "sheets" and they can grow up to several square metres in size and some centimetres thick (Hendrickson 2006). If the sheets fall to the base of the reactor they can block the holes of the distributor plate leading to maldistribution of fluidizing gas and ultimately to loss of fluidization altogether. This necessitates shut-down for clean-up and consequent loss of production. This clearly presents a major problem and much effort has been put into finding solutions (Burdett et al. 2001). A common method of reducing the build-up of electrostatic charges in fluidized beds is to humidify the fluidizing gas but owing to the poisoning effect of water on the organometallic catalysts this cannot be used in the present case.

Various techniques for dissipating electrostatic charges have been proposed by the operating companies and the patent literature contains many examples including the use of special wall coatings (Fulks et al. 1989) and static agents (Goode et al. 1989). The most effective technique however appears to be injecting antistatic agents such as quarternary ammonium salts into the bed to increase the surface

conductivity of the particles (Fischer et al. 2000) although the problem does not appear to have been entirely eliminated in all cases (Moughrabiah et al. 2012).

2.2.1.5 Reactor Modelling

(i) Choi and Ray (1985) analysed the dynamics of a fluidized-bed polyethylene reactor using a two-phase (emulsion and bubble) model and showed them to be prone to unstable behaviour and temperature oscillations. Their work was later extended by McAuley et al. (1994) and further by McAuley et al. (1995) who based their studies on a simplified well-mixed model that showed close similarities with the earlier work. McAuley et al. (1995) first examined the behaviour of the reactor itself and showed the existence of three steady states, a lower at around 300 K which, depending on the catalyst feed rate, is either stable or unstable, a middle state at around 700 K that is always unstable, and an upper state at around 1200 K that is always stable. The only area of interest however is that below the melting point of polyethylene around 400 K. Adding a recycle stream and external cooler to the model showed major differences from the reactor-only case where for a range of catalyst feed rates no steady state was found to exist, limit cycle behaviour being obtained. The authors examined the effect of an ethylene partial-pressure controller and showed that higher partial-pressure set points led to runaway towards a higher-temperature steady state. Further, feed-back temperature control was always essential to maintain steady-state operation.

(ii) Fernandez and Lona (2001) developed a complex model of a polyethylene reactor based on a three-phase description of the system: gaseous bubble phase, gaseous emulsion phase and solids polymer particle phase. They assumed the bubble-phase and emulsion-phase gases to be in plug flow upward and the emulsion-phase solids to be in plug flow downward. Polymer particles were assumed to have a wide size distribution and to segregate according to their size and mass. Their kinetic model assumed the successive steps of catalyst formation, polymerization initiation, propagation, chain transfer, termination and catalyst deactivation, the final model being composed of 165 differential equations. Numerical solution required five sets of iterations; first the system was solved without accounting for the bubble phase in order to evaluate the total monomer consumption. Emulsion-gas and bubble concentrations were then determined followed by overall energy balances. The model showed good agreement with results reported in the literature and in patents. The work was later extended by Fernandez and Lona (2004).

(iii) Kiashemshaki et al. (2006) developed a two-phase model in which the fluidized bed was divided into four sections in series, the gas phase being in plug flow and the emulsion phase completely mixed while Ibrahema et al. (2009) explored a model consisting of four phases: bubbles, cloud, emulsion

and solids. Shamiri et al. (2011) developed a novel two-phase model for propylene polymerization in a fluidized bed but at the time of publication no experimental validation had been obtained.

Despite the considerable body of published work in this area it remains questionable whether two- and three-phase models of the kind described above are capable of giving an adequate description of polyolefin reactors. The Unipol and other similar reactors are known to operate in the turbulent regime where gas bubbles are at best ill-defined and may well be absent altogether as definite entities. It may well be that generalised bubbling/turbulent models such as that proposed by Thompson et al. (1999) are to be preferred for these systems as may be the work of Alizadeh et al. (2004) whose tanks-in-series model of a polyethylene reactor is based on the turbulent model of Cui et al. (2000). Also noteworthy are the two dynamic models described by Secchi et al. (2013). The model of Thompson et al. (1999) treats the turbulent condition as being transitional between the purely two-phase bubbling and slugging regimes and the homogeneous single-phase structure of axially-dispersed plug flow, merging one into the other using the probabilistic averaging of key parameters that vary continuously with superficial gas velocity. In other words the model predicts a smooth transition from two-phase fluidization to single-phase axially-dispersed flow. The model was implemented in the gPROMS software from Process Systems Enterprises Ltd and shows great promise for application to general high-velocity turbulent-flow systems.

2.2.2 n-butane Oxidation to Maleic Anhydride

The main uses of maleic anhydride are for the production of unsaturated polyester resins (ca 41 %), butane diol (14 %), maleic copolymers (8 %) and tetrahydrofuran (7 %); installed world capacity is of the order of 1.2 Mt/a (Chiusoli and Maitlis 2008). As well as being an important industrial solvent tetrahydrofuran in turn is used in the production of the segmented polyurethane spandex and elastane fibres such as Lycra and copolyester elastomers such as Hytrel.

2.2.2.1 Process Background

Traditionally produced by the catalytic oxidation of benzene maleic anhydride is now made almost exclusively by the partial oxidation of n-butane over supported vanadium phosphorus oxide catalysts $(VO)_2P_2O_7$:

$$C_4H_{10} + 3.5O_2 = C_4H_2O_3 + 4H_2O; \Delta H = -1260\,\mathrm{kJ/mol}$$

However a complex network of reactions underlies this simple stoichiometry, butene, butadiene and furan having been suggested as intermediates while carboxylic acids and oxides of carbon are also formed in side reactions.

Both multi-tubular fixed-bed and fluidized-bed reactors are widely employed. The reaction is highly exothermic and temperature control is important to maintain catalyst activity and selectivity. In multi-tubular fixed-bed systems this is achieved by circulating a heat-transfer medium of molten salts, the hydrocarbon concentration being maintained below the flammability limit of 1.8 mol% n-butane in air. In fluidized beds temperature control is achieved by means of internal cooling coils and feed concentrations of up to 4 mol% n-butane in air are possible due to the flame-arresting properties of the bed particles (Contractor 1999). Axial solids mixing and the associated gas backmixing however result in a significant loss of selectivity. The recent development of a circulating fluidized-bed reactor (CFB) for n-butane oxidation avoids this problem by carrying out the hydrocarbon oxidation step and the catalyst re-oxidation step in two separate but connected sections of a looped system (see below).

2.2.2.2 The Catalyst

The catalyst used in the selective oxidation of n-butane to maleic anhydride is vanadyl pyrophosphate, $(VO)_2P_2O_7$, often referred to as vanadium phosphoprus oxide or VPO. Owing to its commercial importance a great deal has been published on this material in both the scientific and patent literature over the years (e.g. Blum and Nicholas 1982; Contractor et al. 1987; Bergna 1988; Centi 1993; Patience et al. 2007) and special methods have been developed for producing catalyst suitable for use in fluidized-bed reactors. The VPO precursor material is normally made from vanadium pentoxide and phosphoric acid in an organic medium and following filtration and drying is mixed with polysilicic acid as a slurry then spray dried to form microspheroidal particles. For fluidized-bed application the particles must be attrition resistant and this can be achieved by mixing the dried powder with colloidal silica prior to spray drying; however this can cause a significant loss in selectivity (Blum and Nicholas 1982).

Contractor et al. (1987) describe a method for producing an attrition-resistant catalyst suitable for use in the DuPont Circulating Fluidized-bed process. Thus vanadium pentoxide (100 g) is stirred into a mixture of isobutanol (1L) and benzyl alcohol (150 g) and refluxed for 12 h. 85 % phosphoric acid (150 g) is slowly added and again refluxed for 12 h. The precursor product, vanadyl hydrogen phosphate hemihydrate $VOHPO_4 \cdot 0.5H_2O$, is then cooled, filtered, dried and milled to give particles of 1–2 μm which are then slurried with freshly prepared polysilicic acid hydrogel to give a final solid composition containing 10 % silica. The slurry is then spray dried at 250 °C to give microspheres of mean diameter 70 μm with a strong porous layer of SiO_2 on the outer surface (Bergna 1988). In the final stage the microspheres are calcined and activated with air at 6 bar and 390 °C for four hours (Patience et al. 2007). The particles have a thin coating of silica that

is durable but porous to reactants and products. The catalytic reaction of n-butane over vanadyl pyrophosphate is complex being a 14-electron oxidation involving the abstraction of 8 hydrogen atoms and the insertion of three oxygen atoms the processes occurring entirely on the adsorbed surface. Despite much research (Centi 1993) there is still uncertainty as to the nature of the active centre responsible for the catalysis but it is widely accepted that the process involves a redox reaction according to the Mars-van Krevelen mechanism (Mars and van Krevelen 1954) in which the V^{5+} oxidation state becomes reduced to V^{4+}. Industrial practice is to reoxidise the V^{4+} species on the catalyst surface with molecular oxygen either by co-feeding with the alkane or by regenerating in a separate unit. From limited data on industrial catalysts Centi (1993) concluded that the stable active catalyst is not fully achieved until the butane oxidation has been carried out for 200–500 h; such catalysts are said to be "equilibrated".

Mills et al. (1999) studied the redox kinetics of $VOPO_4$ phases with n-butane and air and showed that the reduction stage leading to the formation of maleic anhydride could be described by a rate expression first order in n-butane and approximately one-third order in the concentration of lattice oxygen. They also showed that during reduction the lattice oxygen species on the catalyst surface react with n-butane thereby establishing a positive gradient for diffusion of sub-surface oxygen to the surface. In the regeneration stage the depleted surface oxygen sites are replaced by oxygen from the air. The kinetic parameters determined by Mills et al. (1999) were applied by Roy et al. (2000) in modelling the riser reactor of the DuPont CFB process (see below).

2.2.2.3 Mitsubishi Process

A commercial plant with a nameplate capacity of 18,000 t/a of maleic anhydride was put into operation in 1970. A schematic flow diagram of the process is shown in Fig. 2.2 (Contractor and Sleight 1987) and an outline of the reactor in Fig. 2.3 (Kunii and Levenspiel 1991).

The feed was the crude C–4 fraction from a naphtha cracker and the reacted gases were fed to a quench tower where the anhydride was absorbed in water to form an aqueous solution of maleic acid and distilled to give the final product. The reactor itself was 6 m in diameter and 16 m high and operated at 400–500 °C and 4 bar pressure. The bed was fluidized with air and the vaporized hydrocarbon feed introduced through a specially designed distributor with hundreds of nozzles (Kunii and Levenspiel 1991). The vessel contained vertical cooling coils generating high-pressure steam; the coils were also believed to restrict gas backmixing and hence to increase catalyst selectivity although work by DuPont proved this to be ineffective. The catalyst was a silica-supported VPO with a size range of 20–200 μm.

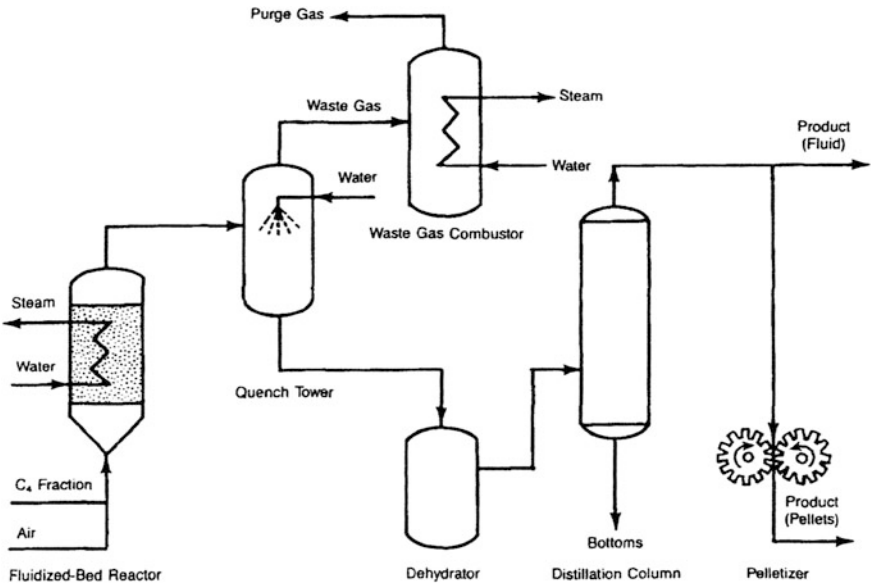

Fig. 2.2 Mitsubishi process for the production of maleic anhydride (Contractor and Sleight 1987)

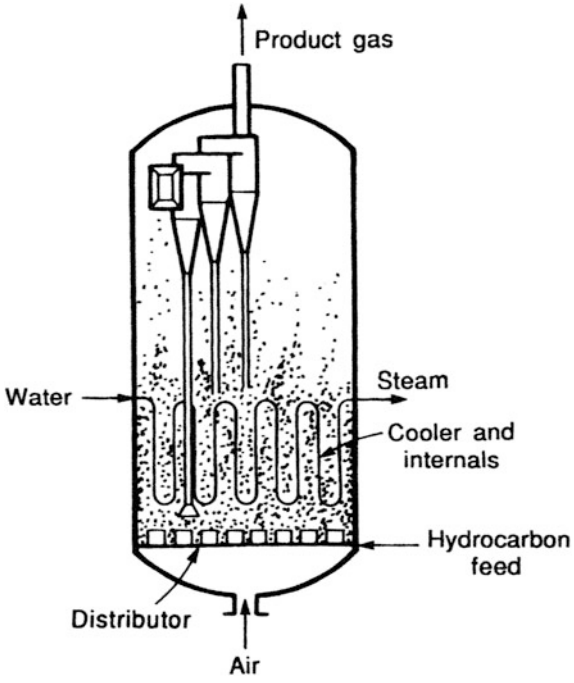

Fig. 2.3 Reactor for the Mitsubishi maleic anhydride process (Kunii and Levenspiel 1991)

2.2.2.4 ALMA Process

ABB Lummus/Lonza under the brand name ALMA have developed a process using a bubbling bed configuration similar to that of Mitsibishi (Fig. 2.3) (Contractor and Sleight 1987; Dente et al. 2003). The reactor is 7 m in diameter and operates at bed temperatures of the order of 240 °C and pressures of 2–4 bar; the n-butane concentration is 4–5 % v/v. The n-butane conversion exceeds 80 % but molar yields of maleic anhydride are limited to 50–55 % (Dente et al. 2003).

The reactor performance is discussed further below.

2.2.2.5 DuPont Circulating Fluidized-Bed Process

The underlying principle of this process was to separate into two reactors the n-butane oxidation step and the reoxidation step of the reduced catalyst, analogous to the cracking-regeneration stages of the FCC process. The VPO catalyst thus acts as an oxygen carrier for the conversion. The process was developed by DuPont over a period of some 20 years from laboratory-scale riser reactors through a pilot plant to a full-scale commercial plant situated at Asturias in northern Spain. The history of the development has been documented in a number of publications (e.g. Contractor and Sleight 1987; Contractor 1999; Patience and Bockrath 2010).

The pilot plant, a scaled down version of the projected commercial unit, consisted of five vessels: 0.3 m × 6 m fast fluidized bed, 0.15 m × 24 m riser, 0.44 m diameter riser stripper, 0.53 m diameter catalyst regenerator, 0.44 m diameter regenerator stripper (Fig. 2.4).

The fast-bed section of the commercial reactor designed on the basis of the pilot-plant results is shown diagrammatically in Fig. 2.5. Recycle gas and fresh n-butane were fed into the bed through a grid-plate distributor at rates of between 0.43 and 0.93 m/s. Owing to the high oxygen demand of the reaction additional oxygen was introduced into the fast bed via three rows of spargers situated below two banks of cooling coils. Regenerated catalyst entered the bed from a slanted standpipe that changed from a circular geometry 1.2 m in diameter at the exit of the regenerator to an oval geometry at the inlet to the fast bed; the bed itself was 4.2 m in diameter and 11.5 m tall. The gas-solid suspension exited the fast bed into the 1.8 m × 28.5 m riser where it passed in plug flow to a rough-cut cyclone then to a stripper and thence to an external cyclone. The product gases passed to a water absorber where the anhydride product was converted to maleic acid a large fraction of the effluent gases being recycled to the fast bed. The maleic acid solution was then hydrogenated to give tetrahydrofuran the final product. On separation from the product gases the VPO catalyst was passed from the stripper to the regenerator, a 4.0 m × 16 m turbulent-flow bed fluidized with air and fitted with horizontal cooling coils. The catalyst inventory in the system was 175 tonnes and solid circulation rates of up to 7000 tonnes/h were achieved. At these high circulation rates with the catalyst flowing through the cyclone, between slide valves and cooling coils a certain degree of attrition was inevitable. Based on the pilot-plant

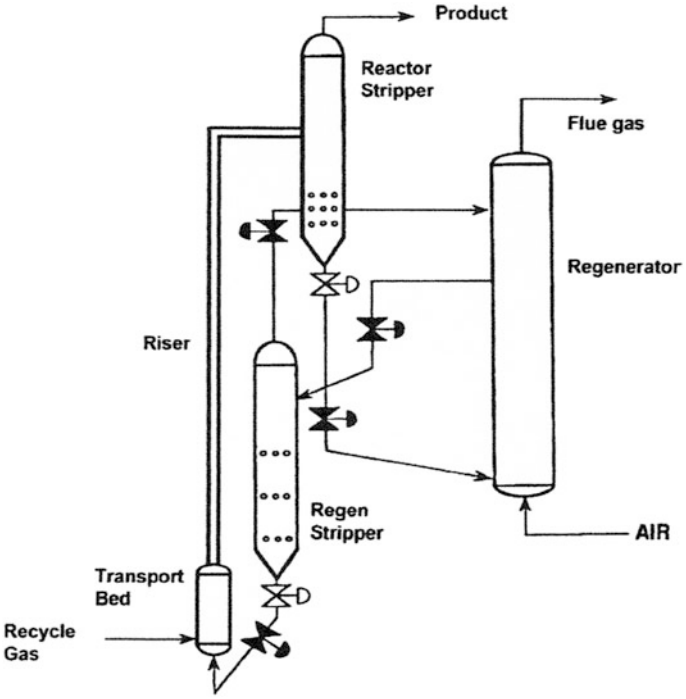

Fig. 2.4 Pilot-plant configuration for the DuPont CFB process (Patience and Bockrath 2010)

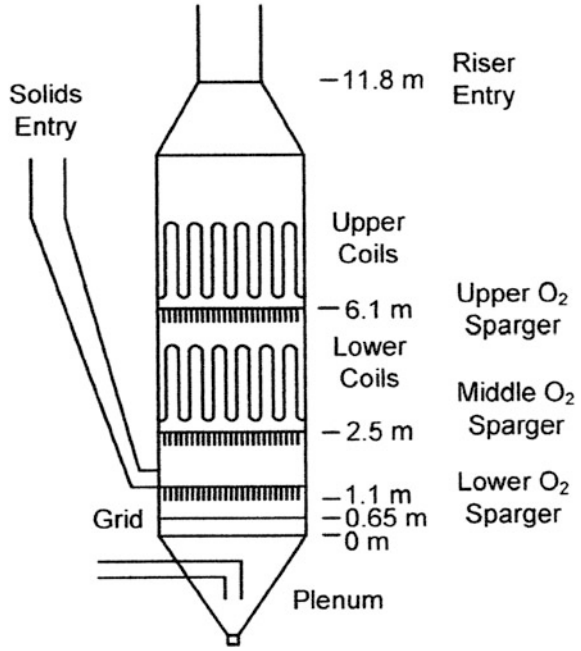

Fig. 2.5 Reactor for the DuPont CFB process (Patience and Bockrath 2010)

performance attrition rates of 5–15 kg/h were expected but lower values in the region of 1.0 kg/h were obtained in practice (Patience and Bockrath 2010).

Some of the operating problems that were never completely solved included incomplete regeneration of the catalyst which necessitated extra oxygen being fed to the fast bed, poor radial distribution of solids in the fast bed and backflow of gas from the fast bed to the regenerator standpipe. Nevertheless the plant operated for a decade after its start-up in 1996 before being finally shut down and dismantled.

2.2.2.6 Reactor Modelling

(i) Moustoufi et al. (2001) studied the performance of a fluidized-bed n-butane-oxidation reactor using three different models:

(a) A simple two-phase model in which all the reaction takes place in the emulsion phase
(b) A so-called "dynamic" two-phase model that considers some reaction to occur in the bubble phase as well as in the emulsion
(c) A model in which the solids are assumed to be uniformly distributed in the bed with a constant voidage the gas passing through in plug flow.

The reaction kinetics used for the model predictions were based on the work of Centi et al. (1985) who determined the oxidation-rate parameters from isothermal steady-state fixed-bed reactor data and proposed the following triangular reaction network where MAN indicates maleic anhydride:

$$\begin{aligned} \text{n-C}_4\text{H}_{10} + 3.5\text{O}_2 &= \text{MAN} + 4\text{H}_2\text{O} \\ \text{MAN} + 4.5\text{O}_2 &= 4\text{CO}_2 + \text{H}_2\text{O} \\ \text{n-C}_4\text{H}_{10} + 6.5\text{O}_2 &= 4\text{CO}_2 + 5\text{H}_2\text{O} \end{aligned}$$

The corresponding rate equations are:

$$r_1 = r_{MAN} = \frac{k_1 K_B c_B c_O^{\alpha}}{1 + K_B c_B} \tag{2.1}$$

$$r_2 = r_{CO_2} = k_2 c_O^{\beta} \tag{2.2}$$

$$r_3 = -r_{MAN} = k_3 c_{MAN} \left(\frac{c_O^{\gamma}}{c_B^{\delta}} \right) \tag{2.3}$$

where r_1 is the rate of formation of maleic anhydride from n-butane, r_2 the rate of formation of CO_2 from n-butane and r_3 the rate of formation of CO_2 from maleic anhydride. The kinetic parameters are shown in Table 2.1.

Results of the computer simulations showed that the plug-flow model predicts higher conversions at higher gas velocities than the two-phase models while

Table 2.1 Empirical kinetic parameters (Moustafi et al. 2001)

Parameter	Value	Units
k_1	6.230×10^{-7}	$\text{mol}^{1-\alpha}\ \text{L}^{\alpha}/(\text{g s})$
k_2	9.040×10^{-7}	$\text{mol}^{1-\beta}\ \text{L}^{\beta}/(\text{g s})$
k_3	0.966×10^{-7}	$\text{mol}^{\gamma-\delta}\ \text{L}^{1-\delta-\gamma}$ (g s)
K_B	2616	mol/L
α	0.2298	
β	0.2298	
γ	0.6345	
δ	1.151	

conversion of n-butane and yield of maleic anhydride both decreased with increasing gas velocity. The results also showed the conversion to decrease with increasing n-butane feed concentration although the selectivity to maleic anhydride was higher at lower n-butane concentrations.

(ii) Dente et al. (2003) developed a bubbling-bed model to describe the operation of the reactor employed in the ALMA process referred to above. Figure 2.6 gives an outline of the reactor geometry and the structure of the reactor model. The model was based on one version of the two-phase model of Davidson and Harrison (1963) in which:

(a) emulsion-phase gas is completely mixed
(b) bubble-phase gas is in plug flow
(c) interphase mass transfer occurs by a combined process of molecular diffusion and throughflow
(d) reaction occurs only in the emulsion phase at an experimentally-determined rate.

Dente et al. first measured the reaction kinetics of the system by means of a tubular microflow reactor loaded with a commercial VPO catalyst, analysing the data on the basis of a scheme comprising five parallel reactions in which n-butane was oxidised to maleic anhydride, acrylic acid, acetic acid, CO and CO_2 and three consecutive reactions in which the anhydride and the two organic acids were oxidised to CO and CO_2.
The Davidson-Harrison model gives the reactant concentration in the emulsion phase as:

$$C_{Ae} = \frac{C_{A0}(1 - f_b e^{-K_{be}})}{1 - f_b e^{-K_{be}} - k'} \tag{2.4}$$

and in the bubble phase as:

$$C_{Ab} = C_{Ae} + (C_{A0} - C_{Ae}) e^{-K_{be}} \tag{2.5}$$

where C_{A0} is the initial concentration of reactant, f_b the bubble-phase gas fraction, K_{be} the interphase mass-transfer coefficient (bubble to emulsion) and k' the appropriate reaction rate coefficient. Dente et al. calculated f_b from bubble sizes and gas velocities as reported by Kunii and Levenspiel (1991) and interphase mass-transfer coefficients (bubble-to-cloud, K_{bc}, cloud-to-emulsion, K_{be}) again from Kunii and Levenspiel (1991):

$$K_{bc} = 4.5\frac{u_{mf}}{d_b} + 5.85\left(\frac{D_{bc}^{1/2} g^{1/4}}{d_b^{5/4}}\right) \tag{2.6}$$

$$K_{ce} = 6.78\sqrt{\frac{D_{ce}^{1/2} u_b \varepsilon_{mf}}{d_b^3}} \tag{2.7}$$

where d_b is the bubble diameter, D_{bc} is the bubble-cloud diffusion coefficient, D_{ce} is the cloud-emulsion diffusion coefficient, g is gravity, u_b is the bubble rise velocity and ε_{mf} is the emulsion-phase voidage. The model was solved on the basis of the tanks-in-series structure shown in Fig. 2.6 although no indication is given of the number of tanks, N, considered (Fig. 2.6).

Model predictions were compared with daily plant data averaged over a two-year period and expressed in terms of n-butane conversion and maleic

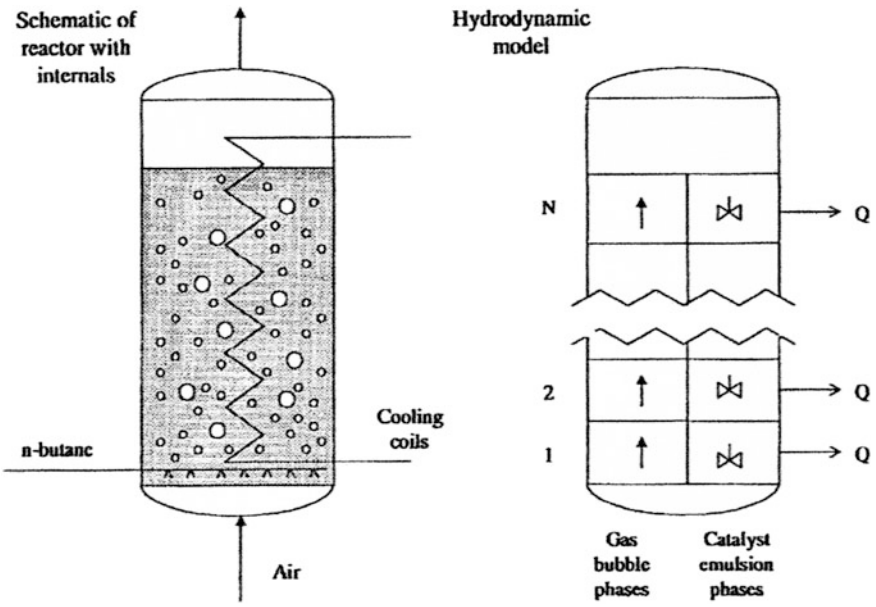

Fig. 2.6 Schematic of the fluidized-bed reactor (diameter 7 m) for the simulation of the ALMA process and discretization sections (Dente et al. 2003)

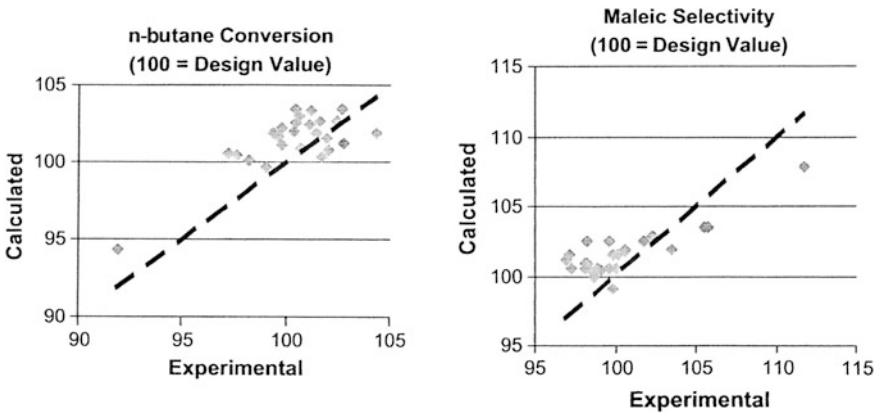

Fig. 2.7 Model predictions versus experimental values for n-butane conversion (Dente et al. 2003

anhydride selectivity, the results being shown in Fig. 2.7. It is clear that the model overestimates both values but the authors conclude that the discrepancies are acceptable.

(iii) Jiang et al. (2003) developed a turbulent-bed model and applied it to the catalytic oxidation of n-butane to maleic anhydride. The model was based on the two-phase concept with a dilute phase containing particles and a dense phase as before. The gas in both phases was assumed to be in plug flow. Since significant particle entrainment occurs in turbulent beds the authors applied a one-dimensional plug-flow model to describe reaction in the freeboard region. The underlying assumptions were (a) the turbulent-bed reactor operates isothermally; (b) catalyst activity is uniform and remains unchanged throughout; (c) reaction takes place in the dense and dilute phases as well as in the freeboard.

A number of authors have developed models of the riser/regenerator system such as that employed in the DuPont process.

(iv) Pugsley et al. (1992) modelled the riser hydrodynamics on the basis of a dense turbulent zone at the base where solids are introduced from the standpipe followed by a zone of fully–developed flow characterised by a core-annular structure with a lean core in which gas and solids flow vertically upwards and a denser gas-solid zone moving downwards at the wall. In view of the smooth exit of the riser to the external cyclone there was no deceleration zone to consider the fully-developed zone being assumed to extend all the way to the outlet. The details of the flow structure were derived from the earlier models of Berruti and Kalogerakis (1989) and Wong et al. (1992). The reaction kinetics incorporated into the model were those of Centi et al. (1985) referred to above. The assumptions made by Pugsley et al. in their computer simulations are listed in Table 2.2.

Table 2.2 Major assumptions for the computer simulations (Pugsley et al. 1992)

The CFB catalytic reactor operates isothermally
Reaction occurs in both the core and annular regions
Catalyst deactivation is the same in both core and annular regions at the same riser
Axial location
Gas input to the annular region is due solely to crossflow of gas from the core
Reaction is chemically controlled
Riser diameter = 0.3 m; riser height = 20 m
The riser is equipped with a smooth exit to the cyclone
G_s = 400–800 kg/(m^{2}s)
U_0 = 4–6 m/s
c_B = 1–50 mol%
T = 573 K
VPO catalyst physical properties (Geldart A)
D_p = 75 μm
ρ_s = 1500 kg/m^3
ε_{mf} = 0.5
U_t = 0.05 m/s

The riser was divided into 100 elements of 20 cm each and from the Berruti and Kalogerakis model core voidage and core radius were found for each element. Mass balance equations for the core and annular regions derived by Patience (1990) were solved for a given inlet concentration of reactants to the first volume element applying the kinetic data of Centi et al. Since the majority of gas was assumed to flow in the core region the reactant concentration in the annulus was assumed to be zero in the first element. The resulting outlet concentrations of reactants and products were then input to the next element and so on to the reactor outlet. The main conclusions of the work were:

- conversion to maleic anhydride decreased but selectivity increased with increasing n-butane feed concentration
- conversion increased at higher solid circulation rates due to increased solids hold-up and better gas-solid contacting
- conversion decreased with increasing gas superficial velocity
- catalyst deactivation had only a slight influence on reactor performance.

(v) Golbig and Werther (1997) carried out an experimental study of n-butane oxidation in a coupled riser-regenerator system using a specially-prepared microspheroidal VPO catalyst. The riser (21 mm i.d., 2880 mm length) was fed with a mixture of n-butane and nitrogen the entrained solids from the riser outlet passing to a stripper and then to the regenerator, a bubbling bed (51–102 mm i.d., 877 mm length) fluidized with an oxygen/air mixture. The freshly regenerated catalyst particles leaving the regenerator were passed to

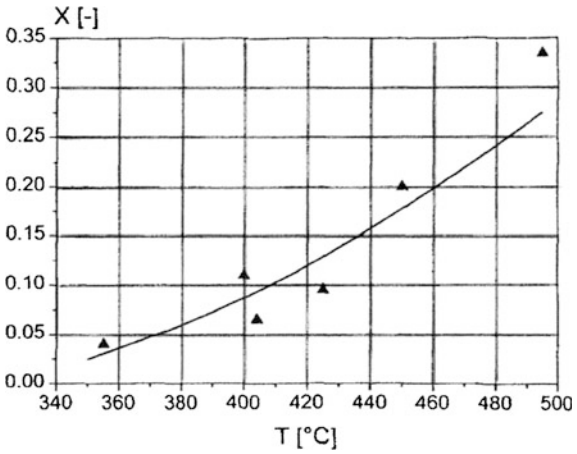

Fig. 2.8 Comparison of the n-butane conversion temperature dependence with model calculations (u_g = 2 m/s; 5 mol% n-butane in the riser; 12–15 mbar pressure drop in the riser; 50 mol% oxygen in the regenerator) (Golbig and Werther 1997)

the riser where they reacted with the n-butane feed to produce MAN, water, CO and CO_2. In the model formulation the riser was represented by two phases: the gas phase and the catalyst phase, mass transfer between the two being described by a previously developed correlation (Vollert and Werther 1994). The regenerator was modelled as a two-phase bubble-emulsion system. In both riser and regenerator the catalyst was assumed to be completely mixed while the gas in both units was in plug flow. Owing to limitations in the supply of catalyst the total operation time of the experimental facility was restricted to some 60 h but sufficient data were collected to enable comparisons to be made with the hydrodynamic model.

Figure 2.8 shows a comparison between n-butane conversion, X, over a range of riser temperatures and model predictions while Fig. 2.9 compares X for a range of n-butane concentrations with the model. The authors conclude

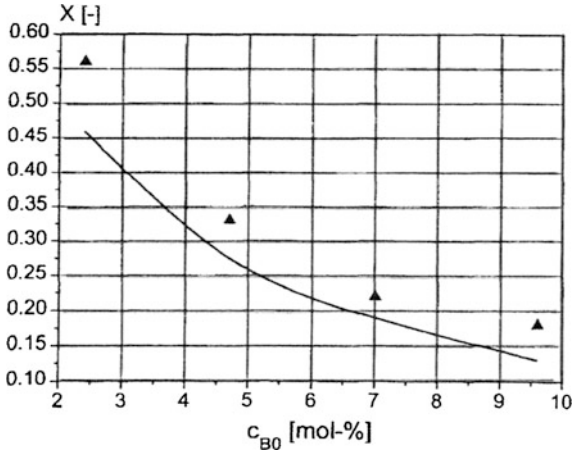

Fig. 2.9 Influence of n-butane feed concentration on the butane conversion—a comparison of measurements and model calculations (500 °C; u_g = 2 m/s; 12–19 mbar pressure drop in the riser; 50 mol% oxygen in the regenerator) (Golbig and Werther 1997)

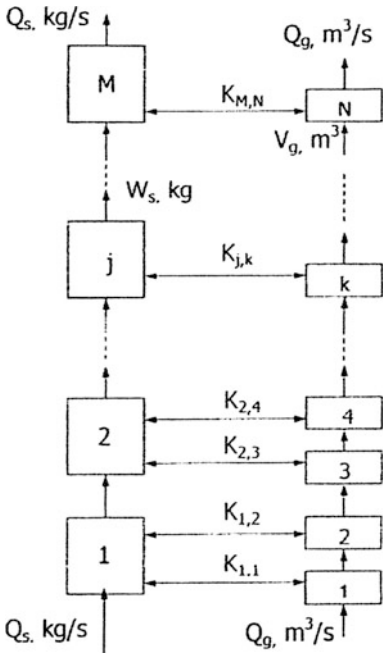

Fig. 2.10 Schematic diagram of the model formulation (Roy et al. 2000)

that the model gives an adequate description of trends in conversion and selectivity to MAN whilst acknowledging that improvements could be made by assuming a more realistic description of the riser in terms of a core-annular structure such as that assumed by Pugsley et al. (1992).

(vi) Roy et al. (2000) based their model on two kinetic schemes: (a) that of Centi et al. (1985) and (b) that of Mills et al. (1999) referred to above. In the model the reaction kinetics were decoupled from the riser hydrodynamics which were described in terms of a series of mixing cells for both solids (M cells) and gas (N cells) with interchange between both (Fig. 2.10). Simulation of a riser as described by Pugsley et al. (1992) was then carried out using the commercial CFD package FLUENT in which the solid and gas phases were assumed to be interpenetrating continua.

The model predictions are shown in Table 2.3 from which it is clear the reactor performance increases the closer the hydrodynamics approach plug flow and that both conversion and yield of maleic anhydride approach asymptotes as the number of compartments increases. The authors conclude that the model of Mills et al. (1999) is the more appropriate for this application since it was measured under conditions that mimic the cyclic exposure of the VPO catalyst to n-butane and oxygen.

In recent years the process simulation tool SolidSim has been developed by eleven institutes from nine German Universities specifically as a means of modelling processes involving fluids and solids (Hartge et al. 2006). The tool

Table 2.3 Effect of mixing pattern on n-butane conversion and MAN yield (Roy et al. 2000)

Number of solid compartments	Number of gas compartments[a]	Conversion of n-butane	Yield of MAN
1	1 (1)	73.3	19.3
	2 (2)	78.1	24.2
	3 (3)	78.6	24.7
	4 (4)	78.6	24.8
	5 (5)	78.6	24.8
	6 (6)	78.6	24.8
2	2 (1)	80.2	27.9
	4 (2)	82.7	28.1
	6 (3)	82.9	28.4
	8 (4)	83	28.5
3	3 (1)	85.9	29.8
	6 (2)	88	31.6
	9 (3)	88.6	32

[a]Numbers in parentheses show the number of gas phase compartments exchanging mass with each solid-phase compartment

was applied by Puettemann et al. (2012a, b) to the selective oxidation of n-butane to maleic anhydride in a riser/regenerator system on both laboratory and industrial scales. The laboratory simulations were based on the earlier work of Goldbig and Werther (1997) while the large-scale simulations used operating data from the DuPont plant referred to above. A major conclusion from the latter simulation was that the solids circulation rates needed to achieve the design yields were unrealistically high, a conclusion in keeping with experience on the plant where the catalyst was never sufficiently regenerated and to compensate it was necessary to inject additional oxygen into the bottom zone of the riser. In the original DuPont experimental unit 50 % of the oxygen came from the regenerator; in the pilot plant this was reduced to some 20 % while in the commercial unit it was often as little as 10 % (Personal Communication). As noted above this was one reason for the process being abandoned after some years of operation.

2.2.3 Propylene Ammoxidation to Acrylonitrile

2.2.3.1 Process Background

Acrylonitrile, a low-boiling (b.p. 77 °C) flammable material, is used extensively in the production of acrylic fibres and resins, ABS rubbers (acrylonitrile-butadiene-styrene) and speciality products. Worldwide production in

2002 was estimated to be 5 Mt/a (Brazdil 2005). It is produced almost exclusively by a fluidized-bed process invented in the late 1950's by the Sohio company (Idol 1959). The process was designated a National Historic Landmark by the American Chemical Society in 1996.

2.2.3.2 Sohio Process

This so-called ammoxidation process involves the reaction between propylene, ammonia and oxygen (air) over a solid catalyst:

$$CH_2=CHCH_3 + NH_3 + 3/2O_2 = CH_2=CHCN + 3H_2O; \Delta H = -515\,kJ/mol$$

In addition, side reactions occur leading to the formation of HCN, acetonitrile, acrolein and oxides of carbon as a result of which the overall enthalpy of reaction is in the region of 670–730 kJ/mol (Kunii and Levenspiel 1991). HCN and acetonitrile are important co-products of the process and are separated from the product stream for further processing. Fluidized-bed operation with cooling coils immersed in the bed enables the heat of reaction to be controlled and bed temperatures to be maintained within the required range of 400–460 °C. Furthermore the flame-quenching action of the moving bed particles enables reactants and products to be processed without hazard despite the wide flammability limits of the organic components in air (Sax 1975).

A typical reactor layout is shown in Fig. 2.11.

Reactor diameters are in the range 3–8 m and are operated at 1.3–2 bar pressure. Air is fed into the unit through a bottom distributor while a mixture of propylene and ammonia enters through sparger pipes with downward-pointing orifices located below the in-bed cooling coils which are fed with water to generate high-pressure steam used to drive the air compressor and for downstream applications. The molar feed ratio of propylene/ammonia/air is 1:1.15:10 giving a minimum excess of ammonia over propylene with about 10 % excess air with respect to propylene (Jiang et al. 2003). To maintain a good quality of fluidization multiple internal cyclones maintain the bed-particle size in the range 10–200 μm with the proportion of fines (<44 μm) being 20–40 %. The oxygen-rich region between the air distributor and the sparger pipes serves to burn off carbon deposits on the catalyst and to reoxidize its surface thereby maintaining the lifetime of the catalyst for prolonged periods (Kunii and Levenspiel 1991). Gas velocities are in the range between 0.4 and 0.5 m/s indicating turbulent-regime flow. Trays or screens can be placed horizontally to reduce gas backmixing and so to improve performance. Gas residence time in the reactor is in the optimal range of 5–10 s resulting in almost 100 % per-pass conversions of propylene with selectivities to acrylonitrile of around 80 % (Dimian and Bildeac 2008).

The use of propane as an alternative feedstock to the more expensive propylene has been discussed in recent years in both the scientific literature (Centi et al. 1993; Fakeeha et al. 2000; Dimian and Bildeac 2008) and in patents (Glaeser et al. 1989).

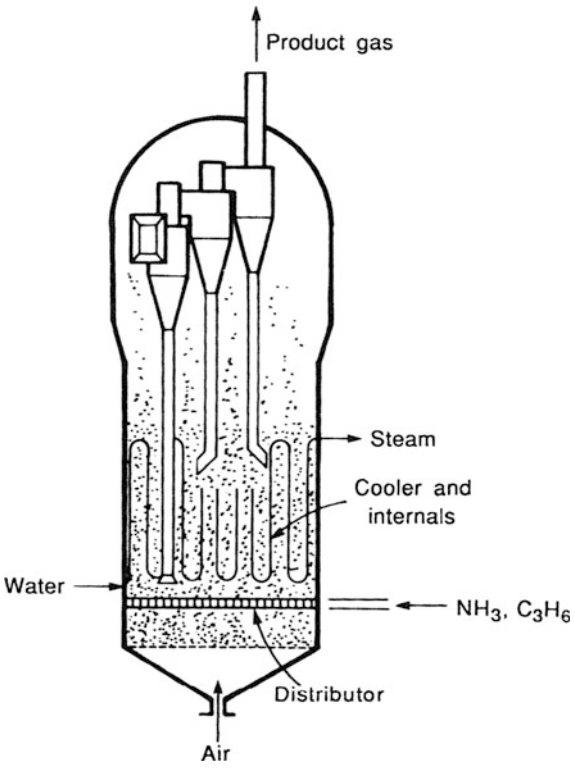

Fig. 2.11 Schematic of a Sohio ammoxidation reactor (Kunii and Levenspiel 1991)

Catalysts similar to those used in the Sohio process have been proposed, some containing vanadium and antimony, but selectivities to acrylonitrile have generally been lower at around 60 % with conversions of 50 %. This inferior performance coupled with the problem of higher temperature operation (500–550 °C) producing a wider range of by-products has proved insufficient to justify the massive replacement costs of existing technologies.

2.2.3.3 Catalysts

The catalyst employed in the original Sohio process was bismuth phosphomolybdate supported on microspheroidal silica particles in which the bismuth component initially activates the propylene molecule by abstraction of a hydrogen atom to give an adsorbed π-allyl intermediate. The function of the molybdenum is thought to be to activate the ammonia molecule to generate NH species which are then inserted into the π-allyl group to form acrylonitrile precursors. This is followed by rearrangement, additional hydrogen abstraction and desorption of the resulting acrylonitrile. The complex sequence of reactions has been described in detail by Grasselli (1986, 1999) and Hanna (2004). Catalysts currently in use are

multicomponent materials containing a range of metals such as iron, nickel, cobalt, magnesium, caesium and potassium (Grasselli 1999). The iron acts as a redox couple ($Fe^{3+/2+}$) transferring lattice oxygen to the Bi–O–Mo active site. The Fe^{2+} surface sites are stabilised by divalent elements such as Ni, Co, Mg and Mn to form stable molybdates that are isostructural with Fe^{2+} molybdates. Alkali metals such as potassium serve to neutralise acidic cracking sites on the catalyst surface. These multicomponent formulations give superior performance in terms of activity and selectivity over the original version, in most cases giving an acrylonitrile yield in excess of 75 mol% based on propylene feed (Grasselli 1999).

2.2.3.4 Reactor Modelling

Kunii and Levenspiel (1991) considered the ammoxidation of propylene on the basis of the following reaction scheme:

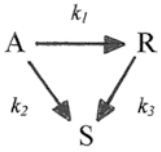

where A = propylene, R = acrylonitrile, S = HCN, CO, CO_2 etc., k_1, k_2 and k_3 being the corresponding reaction rate coefficients. The system was modelled using the authors' "bubbling bed" model (Kunii and Levenspiel 1969) and calculations were carried out to determine the dimensions and operating parameters of a commercial-scale reactor packed with an array of vertical cooling tubes. The model gives the fraction of propylene unconverted leaving the reactor as:

$$\frac{C_A}{C_{A0}} = \exp\left(-k_{f12}\tau\right) \tag{2.8}$$

and the conversion, X_A as:

$$X_A = 1 - \frac{C_A}{C_{A0}} \tag{2.9}$$

where k_{f12}, the effective rate coefficient for propylene conversion, is given by:

$$k_{f12} = \frac{\delta}{1-\varepsilon_f}\left[\gamma_b k_{12} + \frac{1}{\frac{1}{K_{bc}} + \frac{1}{\gamma_c k_{12} + \frac{1}{\frac{1}{K_{ce}} + \frac{1}{\gamma_e k_{12}}}}}\right] \tag{2.10}$$

where: $k_{12} = k_1 + k_2$

K_{bc} = bubble-to-cloud mass transfer coefficient
K_{ce} = cloud-to-emulsion mass transfer coefficient
γ_b = fraction of solids in bubbles
γ_c = fraction of solids in the cloud
γ_e = fraction of solids in the emulsion
δ = bubble volume fraction
ε_f = emulsion-phase voidage

K_{bc} and K_{ce} are found from Eqs. (2.6) and (2.7). u_0 and u_b are the superficial gas velocity and the bubble rise velocity respectively while:

$$\delta = \frac{u_0}{u_b} \tag{2.11}$$

$$\delta(\gamma_b + \gamma_c + \gamma_e) = \left(1 - \varepsilon_{mf}\right)(1 - \delta) \tag{2.12}$$

and

$$\gamma_b, \gamma_c, \gamma_e = \frac{volume\ of\ solids\ dispersed\ in\ b, c, e\ respectively}{volume\ of\ bubble} \tag{2.13}$$

In Eq. (2.8) τ is a gas residence time defined as:

$$\tau = \frac{L_f\left(1 - \varepsilon_f\right)}{u_0} \tag{2.14}$$

where L_f is the bed height, and the average bed voidage, ε_f is:

$$\varepsilon_f = \delta + (1 - \delta)\varepsilon_e \tag{2.15}$$

ε_e being the emulsion-phase voidage.

The model was solved for a number of values of the reaction rate coefficients, conversions and selectivities being plotted in Fig. 2.12 the results then being applied to calculate the overall dimensions of a commercial-scale unit to produce 50,000 tons of acrylonitrile per 334-day year with a propylene conversion of 95 % and a selectivity to acrylonitrile of at least 65 %. The heat of reaction was to be removed via an array of vertical heat exchanger tubes 0.08 m in diameter and 7 m in length that controlled the bed temperature at 460 °C; the bed pressure was to operate at a pressure of 2.5 bar. Applying heat-transfer correlations from the literature the required number of tubes was calculated to be 296 arranged in a square array with a pitch of 0.323 m the resulting bed diameter being 7.18 m.

The calculations are a good example of the application of a fluidized-bed reactor model to the design of a full-scale reactor and of the physical and chemical data required to carry out the design.

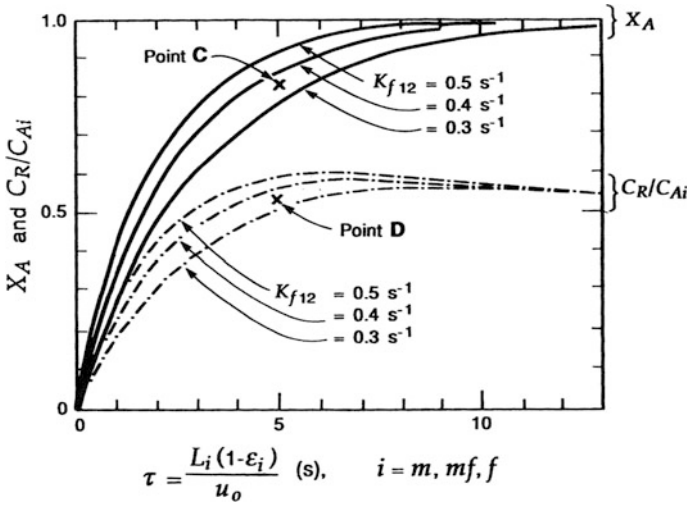

Fig. 2.12 Comparison of calculated lines with experimental data for propylene ammoxidation (Kunii and Levenspiel 1991)

2.2.4 Vinyl Chloride Monomer (VCM)

Vinyl chloride, the precursor material for polyvinyl chloride (PVC), is made by the thermal cracking of ethylene dichloride (1,2-dichloroethane) in a tubular reactor at 450–600 °C and 10–35 bar:

$$CH_2ClCH_2Cl \rightarrow CH_2=CHCl + HCl; \Delta H = 72.6\,kJ/mol$$

The ethylene dichloride itself is made by (a) the direct chlorination of ethylene in the liquid phase with itself as solvent and ferric chloride (Fe(III) chloride) as catalyst at 40–100 °C and 1–10 bar:

$$CH_2=CH_2 + Cl_2 \rightarrow CH_2ClCH_2Cl;\ \Delta H = -180\,kJ/mol$$

and (b) the oxychlorination reaction in which HCl recovered from the pyrolysis stage is reacted with ethylene, air or oxygen in a fluidized-bed reactor at 220–245 °C and 2.5–6 bar:

$$CH_2=CH_2 + HCl + {}^1/_2O_2 = ClCH_2CH_2Cl + H_2O; \Delta H = -237.3\,kJ/mol$$

Combining the three processes of direct chlorination, ethylene dichloride pyrolysis and oxychlorination leads to the so-called "balanced" process with no net consumption or production of HCl. The highly exothermic oxychlorination reaction

is catalysed by alumina-supported copper oxide and strict temperature control is necessary to prevent (i) catalyst agglomeration, (ii) ethylene combustion, (iii) over chlorination of the ethylene dichloride product. The catalyst is a Geldart Group A material, the fluidized-bed reactor having many features in common with the Sohio ammoxidation reactor shown in Fig. 2.11 (Jazayeri 2003). Isothermal operation is achieved by the use of densely-packed serpentine cooling coils immersed in the bed the material of construction of both reactor and coils being carbon steel (Bolthrunis et al. 2004).

2.2.5 *Vinyl Acetate Monomer (VAM)*

Vinyl acetate, a major industrial chemical with worldwide production in excess of 4.5 Mt/a, is used in the production of polyvinyl acetate, polyvinyl alcohol and a number of other materials for use as adhesives, films and emulsion-based paints. The main production route for VAM is the acetoxylation reaction between ethylene, acetic acid and molecular oxygen in fixed-bed reactors over a catalyst containing palladium, gold and a promoter such as potassium acetate supported on silica:

$$CH_2=CH_2 + CH_3CO_2H + {}^1\!/_2\,O_2 \rightarrow CH_2=CHCO_2CH_3 + H_2O;\ \Delta H = -211.2\,\mathrm{kJ/mol}$$

A typical catalyst of the type introduced by Bayer in the 1960's consists of 0.5–1.5 % Pd, 0.2–1.5 % Au, 4–10 % KOAc on silica in the form of 5 mm diameter spheres operated at 140–180 °C and 5–12 bar pressure.

In late 2001 BP Chemicals, in an attempt to establish a new technology in the field, started up the world's first fluidized-bed process for VAM at their Saltend, Hull facility in the UK with a capacity of 250 kt/a from a single reactor. The advantages of the fluidized-bed for the process were simplicity of design, increased catalyst life (since catalyst deactivation was minimised by the absence of hot spots common in fixed beds), continuous addition of make-up catalyst, and higher production rates since higher oxygen levels could be used without the risk of forming a flammable mixture in the fluidized environment. The Pd/Au-based catalyst was a microspheroidal Geldart Group A material (Baker et al. 2003) in a reactor similar in form to that referred to above for the oxychlorination process for VCM (Fig. 2.17). The plant was operated successfully for a number of years with no reported technical problems. However having been acquired from BP by INEOS in 2008 and owing to a combination of the availability of low-cost imports and a hostile trading environment the process became uneconomic and the plant was shut down in October 2013.

2.2.6 *Gas-to-Liquid Technologies*

Factors such as the volatility of the international oil market and the lack of indigenous sources of crude oil in various countries have prompted the development of processes to produce liquid fuels and chemicals from coal and natural gas. Thus in Germany in the period between the two World Wars two processes, the Bergius process for the production of hydrocarbon fuels by the high-pressure hydrogenation of brown coal and the Fischer-Tropsch process for generating liquid fuels and chemicals from synthesis gas, were developed and commercialised. In the Bergius process finely divided coal was slurried with recycled oil containing an iron catalyst and hydrogenated at 400–500 °C and 20–70 MPa pressure to give a synthetic crude oil. The Bergius process is no longer practiced but variants of the Fischer-Tropsch process have proliferated in countries such as South Africa and China with widespread deposits of coal but little in the way of petroleum or natural gas.

Synthesis gas or "syngas" is made by the steam gasification of coal using, for example, Lurgi dry-ash gasifiers (Dry 1996). Lurgi gasifiers operate under pressure (2–3 MPa) and use a steam/oxygen mixture as the gasifying medium:

$$3C + O_2 + H_2O \rightarrow H_2 + 3CO$$

The feedstock is lump coal which is admitted to the reactor via a pressurised hopper and kept in motion during reaction by means of a rotating grate through which the ash is discharged. The crude syngas is a mixture of mainly H_2, CO, CO_2 and CH_4 the actual compositions depending on the process conditions and the type of coal used. For use in the Fischer-Tropsch process the purified syngas composition should be such that the ratio $H_2/(2CO + 3CO_2)$ is slightly greater than 1.0 (Dry 1996). Where necessary the H_2/CO ratio may be adjusted via the nickel-catalysed water-gas shift reaction:

$$H_2O + CO \leftrightarrow H_2 + CO_2;\ \Delta H = -41\,\mathrm{kJ/mol}$$

The Fischer-Tropsch reaction may be represented by:

$$(2n + 1)H_2 + nCO \rightarrow C_nH_{2n+1} + nH_2O$$

where n is in the range 10–20. The alkane products are largely linear and vary from methane to heavy waxes; the liquid products are suitable as diesel fuel but the gasoline yield is low and of poor quality.

2.2.6.1 Synthol Process

The South African Sasol company have since the mid-1950's operated large-scale units for the production of a range of coal-derived gases and liquids via a

combination of the Lurgi and Fischer-Tropsch processes. In the early years a total of thirteen Lurgi gasifiers were installed each of some 4 m diameter with a total capacity of around 8.2×10^6 m^3/day of raw gas. The gasifiers supplied gas to two Fischer-Tropsch variants, the Arge process and the Synthol process. The Arge plant consisted of five packed-bed reactors producing 18,000 tonnes/year of hydrocarbons. The Synthol plant had two circulating fluidized-bed (CFB) reactors each with a capacity of 65,000 tonnes/year (2200 bbl/d) of hydrocarbons. The original Synthol reactors were designed on the basis of data from 4 and 10 cm diameter pilot-plant units obtained by the Kellogg company in the USA and the decision was taken to build CFB reactors rather than the alternative bubbling beds that had been used unsuccessfully in the previously-mentioned Hydrocol process (Sect. 1.2.1.2). The decision to build CFB reactors "although causing much anguish initially, paid off handsomely in the end" (Duvenhage and Shingles 2002). Here the powdered (Geldart A) iron catalyst is carried upwards in dilute-phase flow by the fluidizing syngas at 3–12 m/s and temperatures initially of around 315 °C but rising as the exothermic synthesis reactions start to occur. Heat is removed in coolers situated in the expanded section of the riser the temperature reaching a maximum of 350 °C in the hopper above the standpipe. After separation of product gases and catalyst in banks of cyclones the catalyst is returned via the hopper and standpipe to be picked up by the incoming syngas to renew the process.

As a consequence of the embargo on the import of oil-based products into South Africa imposed by the OPEC in the early 1970's the Sasol company in association with Badger embarked on a major expansion of the coal-to-oil technology. The result was the construction of eight enormous 60 m tall CFB reactors that started up in 1980; a further eight such units began operation in 1982; the overall dimensions of the reactors are shown in Fig. 2.13.

The CFB reactors and their complex support structures were costly to build and expensive to operate and maintain and during their period of development the company began work on the design of a less expensive system based on the so-called Sasol Advanced Synthol (SAS) turbulent dense-phase fluidized-bed reactor. The first commercial-scale SAS unit based on a 5 m diameter 3000 bbl/d reactor began operation in 1989 followed by an 8 m diameter 11,000 bbl/d unit two years later (Sookai et al. 2001). During 1998/99 the 16 CFB reactors were replaced by four 10.7 m and four 8 m diameter SAS reactors (Duvenhage and Shingles 2002); the dimensions and product yields of the reactors are shown in Fig. 2.13.

Synthol catalyst is a promoted iron powder (Geldart Group A) derived from the millscale produced in steel making. In addition to the Fischer-Tropsch reaction shown above the catalyst promotes a side reaction, the Boudouard reaction, in which CO is decomposed to CO_2 and carbon the latter reacting to form iron carbide on the catalyst surface. This results in a decrease in the particle density of the catalyst which if unchecked would lead to uncontrollable bed expansion and catalyst loss through the cyclones. To counter this carbided catalyst is removed continuously and replaced with fresh material giving an optimum balance between the good flow properties of the used material and the high conversion potential of the fresh (Sookai et al. 2001).

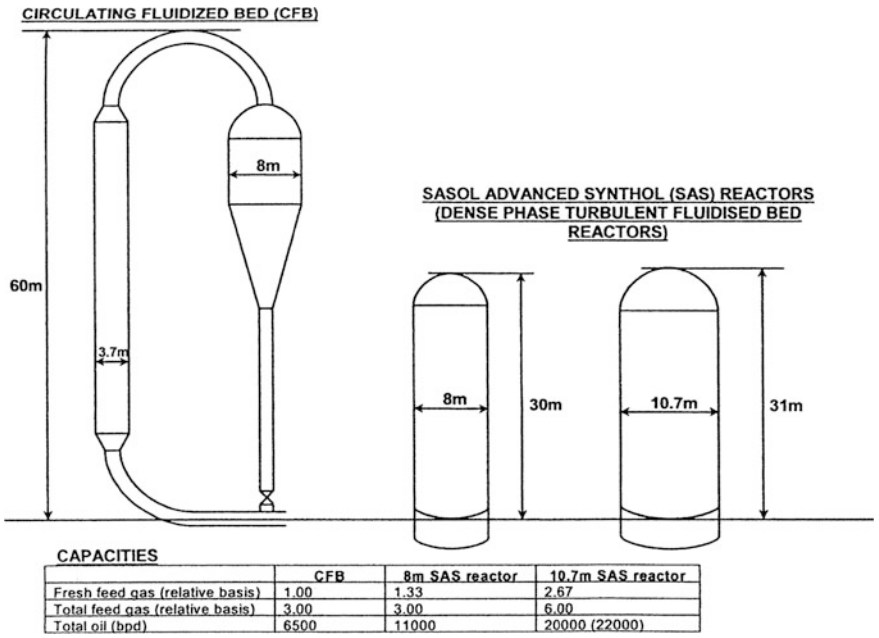

CAPACITIES

	CFB	8m SAS reactor	10.7m SAS reactor
Fresh feed gas (relative basis)	1.00	1.33	2.67
Total feed gas (relative basis)	3.00	3.00	6.00
Total oil (bpd)	6500	11000	20000 (22000)

Fig. 2.13 Size and capacity comparison between Synthol CFB and SAS reactors (Sookai et al. 2001)

Some of the advantages of the SAS units over the CFB units have been set out by Duvenhage and Shingles (2002) as follows:

- higher per-pass conversions
- lower catalyst consumption (by 50 % per ton) of product
- excellent isothermal performance and temperature control
- less maintenance
- greater run stability
- less erosion of critical components and less catalyst attrition

2.2.6.2 Methanol-Based Processes

Driven by the volatility of the market in petroleum products in the 1970's the Mobil company (now ExxonMobil) developed a process for converting methanol to gasoline; the MTG process was first commercialised at Motunui in New Zealand in the mid-1980's. The route to methanol started with the steam reforming of methane in fixed bed reactors over a nickel-based catalyst followed by the water gas shift reaction:

$$CH_4 + H_2O \leftrightarrow CO + 3H_2; \quad \Delta H = +206\,kJ/mol$$
$$CO + H_2O \leftrightarrow CO_2 + H_2; \quad \Delta H = -41\,kJ/mol$$

The product gases were then converted to methanol in fixed beds over a copper catalyst:

$$CO_2 + 2H_2 \leftrightarrow CH_3OH; \quad \Delta H = -92\,kJ/mol$$

the resulting methanol then being dehydrated in a fixed-bed reactor over an alumina catalyst to give an equilibrium mixture of dimethyl ether, methanol and water:

$$2CH_3OH \leftrightarrow CH_3OCH_3 + H_2O$$

The mixture was passed to a series of fixed-bed reactors containing the zeolite catalyst ZSM-5 where it was mixed with recycle gas and converted to a mixture of hydrocarbons and water. The ZSM-5 structure has pores of diameter 5.1–5.6 Å leading to a hydrocarbon product in the C_1–C_{10} range which after downstream treatment yielded gasoline with an octane rating of 92–95. In the MTG stage the catalyst became deactivated by the deposition of coke and was regenerated by burning off with air. The original plant used five swing reactors with one being regenerated off-line at any one time the other four being run in parallel. For economic reasons the Moturui plant was shut down in 1996 but second generation versions of the process (Harandi 1993) have subsequently been introduced and are of particular interest in developing countries such as China which, like South Africa, have large deposits of coal but little crude oil.

A further development of the MTG process is the methanol-to-olefin (MTO) technology being introduced as a source of ethylene and propylene for the burgeoning polymer market. The MTO process originated with the discovery by Union Carbide of a new class of zeolite catalyst, the silicoaluminophosphates (SAPO, particularly SAPO-34) which showed high selectivity to light olefins from methanol. SAPO-34 is made up of narrow pores of diameter 5.1–5.6 Å connected to large cages and leading to a narrow product distribution in the C_1–C_5 range. A number of versions of the process are currently available commercially and some such as the UOP/Hydro MTO process employ fluidized-bed reactor/generator technology for catalyst management (Funk et al. 2013; Chen et al. 2005). Developments of MTG and MTO installations in China have recently been summarised by Minchener (2014). Academic interest in MTO catalysis has been considerable with groups worldwide reporting mechanistic, kinetic and modelling studies (Park and Froment 2004; Gayubo et al.. 2005; Zhou et al. 2008; Kaarsholm et al. 2010).

2.2.7 *Fluidized Catalytic Cracking (FCC)*

2.2.7.1 Process Background

Since its introduction over 70 years ago fluidized catalytic cracking has become the most widespread fluidized-bed process and arguably the most important catalytic process in all industry. Its aim is to convert low-value heavy petroleum distillate fractions into lighter high-value products boiling in the gasoline and light-oil ranges. In terms of throughput catalytic crackers are second only to the atmospheric distillation units on most refineries. On refineries the heavy residue from the primary atmospheric distillation unit is fed to the vacuum distillation column giving vacuum gas oil and a residue boiling in the range 340–560 °C and it is this residue that was the traditional FCC feedstock; modern units however can process a wide variety of feeds including hydro-treated gas oils and deasphalted oils, as well as atmospheric residue (Chen 2003). The primary function of FCC units is to produce gasoline, some 45 % of worldwide production coming either directly or from downstream units such as alkylation plant; middle distillate, light petroleum gas and light olefins for petrochemical conversion are also important products.

Over the years many engineering companies such as UOP, Stone and Webster and Kellogg Brown Root as well as oil companies such as Shell and Exxon/Mobil have developed different versions of FCC systems (Gary and Handwerk 2001) an example being shown in Fig. 2.14.

Although differing in configuration all these versions are based on the same general principles. Cracking is carried out in a vertical riser-reactor at 480–540 °C where hot catalyst is fluidized and carried upwards in plug flow by preheated vaporized feed introduced through atomising nozzles, the catalyst-to-oil ratio normally being in the range 4:1 to 9:1 by weight (Sadeghbeigi 2012). The endothermic cracking reactions occur in the riser over a two-to-four second period and in the process the catalyst becomes deactivated by the deposition of coke (typically 0.4–2.5 wt%) on its surface. Deactivated catalyst flows from the riser into the reactor which acts as a disengaging space and a housing for single- or two-stage cyclones. These deliver the catalyst to a stripper section at the base of the reactor where it is fluidized with steam in a bubbling-bed mode, the stripped vapours passing out overhead with the primary products. Separated catalyst then flows via a standpipe into the regenerator where it is fluidized with air, the coke is burned off at temperatures of 675–730 °C to a typical level of 0.05 wt% and its catalytic activity restored. The cycle of events is completed as regenerated catalyst flows from the regenerator into the riser to resume the process. The flow rate of the catalyst between regenerator and riser is normally regulated by means of a slide- or plug-valve which controls the pressure head necessary for catalyst circulation around the system. Coke combustion raises the catalyst temperature to that required in the cracking reactions so maintaining a heat balance around the system. Cracked products and steam leave from the top of the reactor and pass to a fractionator for separation into four product groups: light gases (C_1–C_4), gasoline (C_5–220 °C),

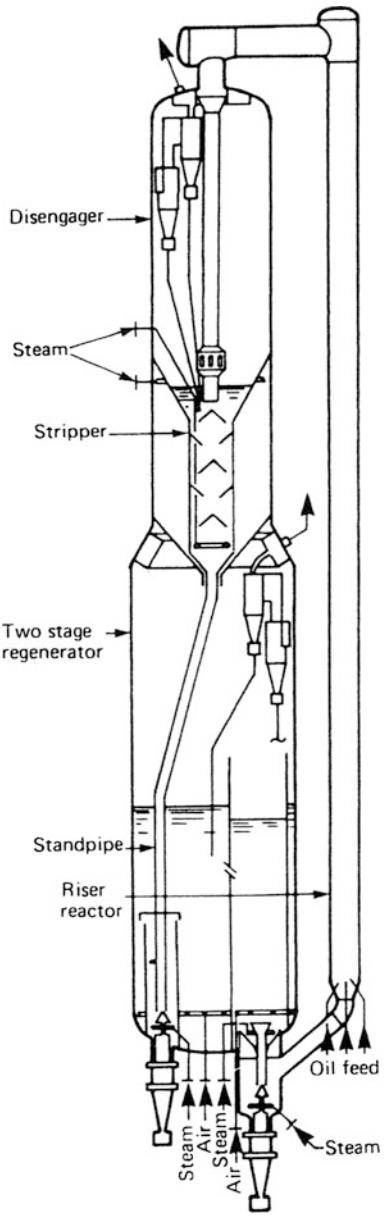

Fig. 2.14 A modern riser cracker

light cycle oil and heavy cycle oil (220–340 °C) and so-called slurry- or decant-oil (340 °C+). Steam and oxides of carbon, sulphur and nitrogen leave from the regenerator. By controlling the flow rates of feed, air and steam a continuous circulation of catalyst is maintained between riser-reactor and regenerator. In modern designs the risers operate in the fast fluidization regime at their lower end

and, owing to the gas expansion caused by the cracking reactions, in dilute transport flow at their upper end; regenerators operate in turbulent-to-fast flow.

2.2.7.2 FCC Catalysts

Modern materials consist of four components: a zeolite, an amorphous silica-alumina matrix, a binder and a filler. The zeolite is the most active component and constitutes 15–50 wt% of the mixture. Zeolites are porous, crystalline aluminosilicates many of which have the general formula $M_{x/n}[(AlO_2)_x(SiO_2)_y] \cdot zH_2O$ where x/n is the number of exchangeable cations, M, of valency n. Those used in catalytic cracking have the structure of the naturally-occurring mineral faujasite but are chemically distinct from it. The basic unit of the faujasite structure is the cubo-octahedron made up of twenty four tetrahedra of either SiO_4^{4-} or AlO_4^{5-} connected through their hexagonal faces to give a unit cell of 192 tetrahedra with an edge length of 24.95 Å. It has an open, cage-like structure with large cavities interconnected by channels of 8–10 Å diameter allowing only smaller molecules to enter. One synthetic form, zeolite X, is made by crystallizing a sodium alumino silicate gel prepared by mixing aqueous solutions of sodium aluminate, sodium silicate and sodium hydroxide. The amorphous gel so formed is crystallized by agitation and heating at 100 °C and the sodium component ion-exchanged with other cations (NH_4^+, Ca^{2+}, La^{3+} etc.) to give the final structure. The Bronstedt- and Lewis-acid sites formed within the cavities are the active centres for the cracking reactions. The amorphous silica-alumina component of the catalyst promotes the cracking of larger hydrocarbon molecules while the binder and filler provide physical integrity and mechanical strength (Chen 2003).

Zeolites containing trivalent rare-earth cations such as La^{3+}, Ce^{3+}, Pr^{3+}, Nd^{3+}, Sm^{3+} are stable at high temperatures and in the presence of steam, rare earth exchanged materials containing less than 0.5 wt% Na_2O being able to withstand high steam concentrations up to 760 °C and thermal treatment up 815 °C. Of even greater importance than their increased activity compared with silica alumina is their greater selectivity to gasoline and their correspondingly lower yields of C_1–C_4 gases and coke (Table 2.4). This is attributed to their higher activity for hydrogen-transfer reactions relative to cracking in their small pore structure.

Of vital importance in determining the flow characteristics of FCC catalysts are particle size distribution (PSD) and the content of fines in the size range <40 μm. PSD's are in the range 10–150 μm with an average of around 70 μm i.e. a typical Geldart Group A material. Maintaining a steady concentration of fines is essential in preserving the flowability of the catalyst, any significant loss through cyclone malfunction seriously inhibiting catalyst circulation rates.

A number of materials act as poisons for cracking catalysts. Nitrogen compounds react with the acid centres and lower catalytic activity while the metal components of heavy oil fractions such as iron, nickel and vanadium deposit on

Table 2.4 Comparison of yield structure for fluid catalytic cracking of waxy gasoil over commercial equilibrium zeolite and amorphous catalysts (Venuto and Habib 1979)

Yields at 80 vol.% conversion	Amorphous high alumina	Zeolite XZ-25	Δ change from amorphous
Hydrogen wt%	0.08	0.04	−0.04
$C_1 + C_2$s wt%	3.8	2.1	−1.7
Propylene vol.%	16.1	11.8	−4.3
Propane vol.%	1.5	1.3	−0.2
Butenes vol.%	12.2	7.8	−4.4
i-Butane vol.%	7.9	7.2	−0.7
n-Butane vol.%	0.7	0.4	−0.3
Gasoline vol.%	55.5	62.0	+6.5
Light fuel oil vol.%	4.2	6.1	+1.9
Heavy fuel oil vol.%	15.8	13.9	−1.9
Coke wt%	5.6	4.1	−1.5
Gasoline octane number	94	89.8	−4.2

catalyst surfaces and increase the formation of gas and coke and reduce the yield of gasoline.

2.2.7.3 Process Chemistry

Hydrocarbon cracking over zeolite catalysts proceeds in the main by endothermic reactions involving carbenium-ion intermediates. Paraffinic molecules crack to produce olefins and smaller paraffins, and cycloparaffins (naphthenes). Aromatic compounds with alkyl side chains are either dealkylated completely to an unsubstituted aromatic and an olefin or partially cracked to a paraffin and an alkenyl aromatic. These primary reactions are followed by secondary processes leading to the final products. Important among these are hydrogen-transfer reactions, say from a naphthene to an olefin giving an aromatic and a paraffin, isomerizations forming iso-paraffins, and condensation reactions of aromatic residues leading to complex polynuclear hydrocarbons and ultimately to coke. Primary carbenium ions tend to isomerise to the more stable secondary and tertiary ions giving the cracked products a high concentration of highly branched molecules.

The cracking of a linear paraffin may be represented as follows.

Reaction is initiated by an interaction between an adsorbed hydrocarbon molecule and a proton from a Bronstedt acid site on the catalyst surface (Fig. 2.15i). Chain propagation follows by the ethyl carbenium ion abstracting a hydride ion from a second paraffin molecule (Fig. 2.15ii). The secondary carbenium ion so formed undergoes a β-scission reaction to form a primary carbenium ion and an olefin (Fig. 2.15iii). The primary carbenium ion formed in Fig. 2.15(iii) may propagate the chain by abstracting a hydride ion from another paraffin molecule as in Fig. 2.15(ii) or it may rearrange to form a more stable secondary ion

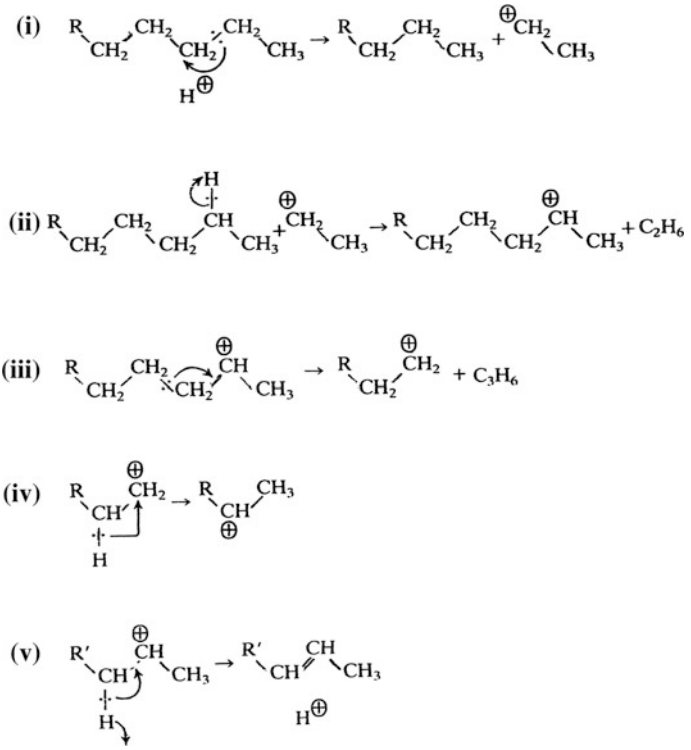

Fig. 2.15 Mechanism of catalytic cracking (Yates 1983)

(Fig. 2.15iv) which may then react as before. Chain termination occurs through donation of a proton back to the catalyst surface (Fig. 2.15v). Reactions of cycloparaffins follow a similar pattern.

The chemistry of catalytic cracking reactions was reviewed extensively by Venuto and Habib (1979) and by Sadeghbeigi (2012).

2.2.7.4 Operating Conditions and Heat Balance

The independent variables that define the reactor-regenerator operating conditions are reactor temperature, feed temperature, space velocity, catalyst activity and reactor pressure. The feed rate and air flow rate to the regenerator are set by flow controllers. The feed temperature is set by the fed temperature controller. Reactor temperature is controlled by the regenerator slide valve regulating the catalyst circulation rate (Chen 2003). The most important dependent variables are regenerator temperature, catalyst-to-oil ratio (i.e. catalyst circulation rate) and overall conversion. In the normal adiabatic mode of operation the combustion of coke on the catalyst provides the total heat requirement of the system. A simplified heat

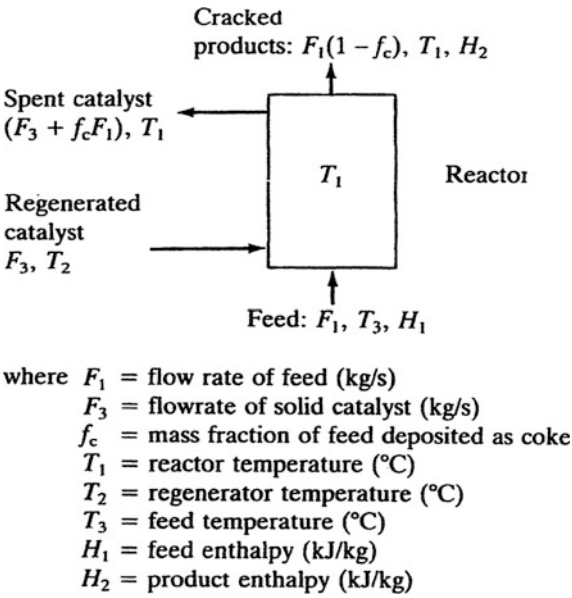

Fig. 2.16 Reactor heat balance (Yates 1983 adapted from Kunii and Levenspiel 1969)

balance on the reactor (ignoring the effects of steam injection in the stripper and losses due to conduction and radiation) gives the following based on Kunii and Levenspiel (1969).

From Fig. 2.16:

$$\begin{aligned}&(\text{heat lost by catalyst}) = (\text{heat of cracking reaction}) + (\text{heat gained by feed})\\ &F_3C_{p,s}(T_2 - T_1) = F_1\Delta H_{crac} + [F_1(1-f_c)]H_2 - F_1H_1\end{aligned} \tag{2.16}$$

$$\text{i.e. } \frac{F_3}{F_1} = \frac{\Delta H_{crac} + (1-f_c)}{C_{p,s}(T_2 - T_1)}\frac{H_2 - H_1}{} \tag{2.17}$$

where $C_{p,s}$ = specific heat capacity of solid catalyst (kJ/kg °C)

ΔH_{crac} = heat of endothermic cracking reaction (kJ/kg feed)

From Fig. 2.17:

$$\begin{aligned}&(\text{heat released by coke combustion}) = (\text{heat gained by gases}) + (\text{heat gained by catalyst})\\ &-\Delta H_{comb}f_cF_1 = [(F_2 + f_cF_1)H_4 - F_2H_3] + F_3C_{p,s}(T_2 - T_1)\end{aligned} \tag{2.18}$$

ΔH_{comb} is the heat of the exothermic coke combustion reaction (kJ/kg coke).

A heat balance on the unit as a whole gives:

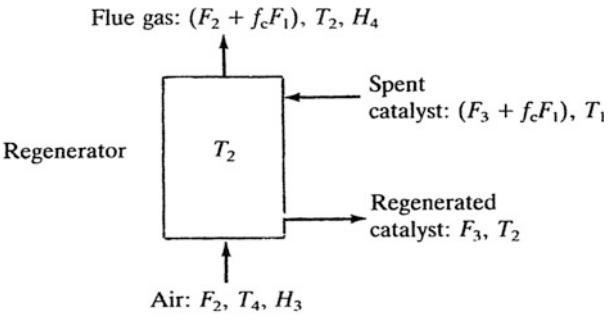

where F_2 = flowrate of air (kg/s)
T_4 = air temperature (°C)
H_3 = air enthalpy (kJ/kg)
H_4 = flue gas enthalpy (kJ/kg)

Fig. 2.17 Regenerator heat balance (Yates 1983 adapted from Kunii and Levenspiel 1969)

$$\text{(heat of coke combustion)} = \text{(heat of cracking reaction)} + \text{(heat gained by feed)} + \text{(heat gained by gases)}$$

from which it follows that:

$$\frac{F_2}{F_1} = \frac{-\Delta H_{comb} - \Delta H_{crac} + [H_1 - (1 - f_c)H_2] - f_c H_4}{H_4 - H_3} \tag{2.19}$$

Assuming the stoichiometry of the combustion reaction to be:

$$\mathrm{C} + \mathrm{O_2} = \mathrm{CO_2} \quad \Delta \mathrm{H} = -404.0\,\mathrm{kJ/mol}$$

$$\frac{f_c F_1}{12} = \frac{0.21 F_2}{1.293 \times 22.4}$$

$$\text{i.e. } \frac{F_2}{F_1} = 11.493 f_c \tag{2.20}$$

Since two of the primary variables in these equations, regenerator temperature and catalyst-to-oil ratio, F_3/F_1, are dependent variables the heat balance calculation requires a trial-and-error approach. For an assumed regenerator temperature, T_2, the catalyst coke content, f_c, may be found from Eqs. (2.19) and (2.20) for given values of H_1, H_2, H_3, T_1, T_3 and T_4. The catalyst-to-oil ratio may then be found from Eq. (2.17) and substituted into Eq. (2.18) and the calculated regenerator temperature compared with the value assumed initially. The highly coupled nature of the reactor-regenerator system is apparent from the foregoing analysis.

Catalyst circulation is determined by the pressure balance around the unit, the rate of circulation being regulated by two slide valves one on the stripper and one on the regenerator.

2.2.7.5 Process Models

Models designed to predict the performance of an industrial process require information of many kinds: the properties and concentrations of the reacting species in the reaction medium, the relevant reaction rate coefficients and stoichiometries as well as a mechanistic description of the fluid flow in the reactor in which the process is carried out. In the case of catalytic cracking the modelling process is complicated by the fact that the feedstock contains thousands of chemical compounds distributed among the various classes—paraffins, naphthenes, aromatics etc. all capable of reacting with the catalyst at different rates and to varying degrees. Historically the approach to the problem of model formulation has been to divide the feed into "lumps" characterised according to one or more correlations based on physical and chemical properties of the hydrocarbon components (Astarita and Sandler 1984). In one such, the "n-d-M" method of Van Ness and Van Westen (1951), refractive index, density and molecular weight are used to identify carbon atoms in the various structures the lumps then being incorporated into a kinetic scheme to predict the performance of the unit. An early example of the method is provided by the work of the Mobil group (Weekman 1968; Voltz et al. 1971) who proposed) a three-lump system comprising unreacted gas oil, A_1, gasoline product, A_2, C_1 to C_4 gases and coke, A_3 combined in the following way:

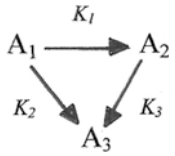

where the K terms represent rate coefficients. Reaction of the gas oil was assumed to be a second-order process while the cracking of the gasoline was assumed to be of the first order. Model equations describing the system for a vapour-phase, plug flow isothermal reactor were developed and tested experimentally against a number of charge stocks, good agreement being found (Voltz et al. 1971). To cater for a wider variety of feedstocks Jacob et al. (1976) developed a 10-lump scheme incorporating coke and light ends, gasoline, light paraffins, heavy paraffins, light naphthenes, heavy naphthenes, light aromatics, light aromatics with side chains and heavy aromatics with side chains. The model has formed the basis for subsequent more complex formulations such as the 19-lump model of Pitault et al. (1994) and the 21-lump model described by Chang et al. (2012). Individual lumps are identified within the boiling ranges obtained by fractionation of the crude, the composition of paraffins (P), naphthenes (N) and aromatics (A) being found from correlations such as that of Riazi (2005):

$$\%X_P \text{ or } \%X_N \text{ or } \%X_A = a + bR_i + cVGC$$

where the X terms represent molar compositions, R_i is the refractive index and VGC is a function of viscosity. The parameters a, b and c vary according to molecular type and boiling range. An additional term accounting for specific gravity can also be included.

Gupta et al. (2007) used a similar approach dividing the feed into 50 lumps, seven of which were the pure components from C_1 to C_5, the remaining 43 being pseudo-components identified according to a complex combination of boiling point and specific gravity. They also modelled the riser as a vertical tube comprising a number of equal-sized two-phase flow compartments in which each phase is well mixed and free from heat- and mass-transfer resistances.

Gao et al. (1999) developed a 3-D two-phase-flow reaction model for FCC risers combining two-phase turbulent flow with 13-lump kinetics. The model, based on the Eulerian two-fluid approach, illustrated the complexity of the feed injection zone at the base of the riser where flow fields, particle concentration, temperature and yield distributions showed significant inhomogeneities in the axial, radial and circumferencial directions. Nevertheless good agreement was found between model predictions and data from a commercial riser reactor.

An alternative approach has been to explore mechanistic models that track the chemical intermediates occurring in the FCC process using transition-state theory to quantify reaction-rate constants for adsorption and desorption at the catalyst surface. Froment has carried out pioneering work in this area (Feng et al. 1993; Froment 2005).

Chang et al. (2012) have reviewed the development since 1985 of so-called "unit-level" models that apply to an entire FCC unit i.e. riser reactor, stripper, regenerator, feed vaporiser, valves and cyclones, each item being described by a sub-model. Details of the sub-models have been given by Han et al. (2004). For a detailed description of the methodology using the Aspen HYSYS Petroleum Refining FCC model the reader is referred to the work of Chang et al. (2012).

References

Alizadeh M, Mostoufi N, Pourmahdian S (2004) Modeling of fluidized-bed reactor of ethylene polymerization. Chem Eng J 97:27–35

Astarita G, Sandler SI (1984) Kinetic and thermodynamic lumping of multicomponent mixtures. Elsevier, Amsterdam

Baker MJ, Couves JW, Griffin KG, Johnston P, McNicol JC, Salem GF (2003) Process for making a catalyst. US Patent 7053024

Bergna HE (1988) US Patent 4,769,477

Berruti F, Kalogerakis N (1989) Modelling the internal flow structure of circulating fluidized beds. Can J Chem Eng 67:1010–1014

Blum PR, Nicholas ML (1982) US Patent 4,317,778

Boland D, Geldart D (1971) Electrostatic charging in gas-fluidized beds. Powder Tech 5:289–297

Bolthrunis CO, Silverman RW, Ferrani DC (2004) Rocky road to commercialization: breakthroughs and challenges in the commercialization of fluidized-bed reactors. In: Fluidization XI. Engineering Conferences International, New York, pp 547–554
Brazdil JF (2005) Acrylonitrile, Ullman's Encyclopedia of industrial chemistry. Weinheim-Wiley-VCH, London
Burdett I D, Eisinger RS, Cai P, Lee KH (2001) Gas-phase fluidization technology for production of polyolefins. In: Fluidization X. United Engineering Foundation, New York, pp 39–52
Centi G (1993) Vanadyl pyrophosphate—a critical overview. Catal Today 16:5–26
Centi G, Fornasari G, Trifiro F (1985) n-butane oxidation to maleic anhydride on vanadium phosphorus oxides: kinetic analysis with tubular-flow stacked-pellet reactor. Ind Eng Chem Proc Des Dev 24:32
Chang AF, Pashikanti K, Liu YA (2012) Refinery engineering: integrated process modelling and optimization. Wiley-VCH, Weinheim
Chen Y-M (2003) Applications of fluidized catalytic cracking. In: Chapter 14 in handbook of fluidization and fluid-particle systems. Marcel Dekker, New York
Chen JQ, Bozzano A, Glover B, Fuglerud T, Kvisle S (2005) Recent advancements in ethylene and propylenre production using the UOP/Hydro MTO process. Catal Today 106:103–107
Chinh J-C, Filippelli MCH, Newton D, Power MB (1998) US Patent 5,733,510
Chiusoli GP, Maitlis PM (2008) Metal catalysis in industrial organic processes. RSC Publishing, Cambridge
Choi K-Y, Ray WH (1985) The dynamic behaviour of fluidized bed reactors for solid catalysed gas phase olefin polymerization. Chem Eng Sci 40:2261–2279
Contractor RM (1999) DuPont's CFB technology for maleic anhydride. Chem Eng Sci 54:5627–5632
Contractor RM, Sleight AW (1987) Maleic anhydride from C-4 feedstocks using fluidized-bed reactors. Catal Today 1:587–607
Cui HP, Mostoufi N, Chaouki J (2000) Characterization of dynamic gas-solid distribution in fluidized beds. Chem Eng J 79:135–143
Davidson JF, Harrison D (1963) Fluidised particles. Cambridge University Press, Cambridge
Dente M, Pierucci S, Tronconi E, Cecchini M, Ghelfi F (2003) Selective oxidation of n-butane to maleic anhydride in fluid-bed reactors: detailed kinetic investigation and reactor modelling. Chem Eng Sci 58:643–648
Dimian AC, Bildeak CS (2008) Acrylonitrile by propene ammoxidation. In: Chemical process design: computer-aided case studies, pp 313–338
Dry ME (1996) Practical and theoretical aspects of the catalytic Fischer-Tropsch process. Appl Catal A 138:319–344
Duvenhage DJ, Shingles T (2002) Synthol reactor technology development. Catal Today 71:301–305
Fakeeha AH, Solimam MA, Ibrahim AA (2000) Modelling of a circulating fluidized-bed for ammoxidation of propane to acrylonitrile. Chem Eng Proc 39:161–170
Feng W, Vynckier E, Froment GF (1993) Single event kinetics of catalytic cracking. Ind Eng Chem Res 32:2997
Fernandez FAN, L:ona LMF (2004) Multizone circulating reactor modelling for gas-solid polymerization: 1 reactor modelling. J Appl Polym Sci 93(3):1042–1052
Fernandez FAN, Lona LMF (2001) Heterogeneous modelling for fluidized-bed polymerization reactor. Chem Eng Sci 56:963–969
Fischer D, Frank H, Lux M, Hingman R, Schweier G (2000) US Patent 6,022,837
Froment GF (2005) Single event kinetic modelling of complex catalytic processes. Catal Rev Sci Eng 47:83–124
Fulks BD, Sawin SP, Aikman CD, Jenkins JM (1989) US Patent 4,876,320
Funk GA, Myers D, Vora B (2013) A Different Game Plan. Hydrocarbon engineering, December
Gao J, Xu C, Lin S, Yang G, Guo Y (1999) Advanced model for turbulent gas-solid flow and reaction in FCC risers. AIChE J 45:1095–1113

Gary JH, Handwerk GE (2001) Petroleum refining: technology and economics, 4th edn. Marcel Dekker, New York
Gayubo AG, Aguayo AT, Alonso A, Atutxa A, Bilbao J (2005) Reaction scheme and kinetic modelling for the MTO process over SAPO-18 catalyst. Catal Today 106:112–117
Glaeser LC, Brazdil JF, Toft MA (1989) US Patent 4,837,233
Goldbig KG, Werther J (1997) Selective synthesis of maleic anhydride by spatial separation of n-butane oxidation and catalytic reoxidation. Chem Eng Sci 52:583–595
Goode MG, Hasenberg DM, McNeil TJ, Spriggs TE (1989) US Patent 4,803,251
Grasselli RK (1999) Advances and future trends in selective oxidation and ammoxidation catalysts. Catal Today 49:141–153
Gupta RK, Kumar V, Srivastava VK (2007) A new generic approach for the modelling of fluid catalytic cracking riser reactor. Chem Eng Sci 62:4510–4528
Han IS, Riggs JB, Chung CB (2004) Modelling and optimization of a fluidized catalytic cracking process under full and partial combustion modes. Chem Eng Proc 43:1063–1084
Hanna TA (2004) The role of bismuth in the Sohio process. Coord Chem Revs 248:429–440
Harandi MN (1993) US Pstent 5,177,279
Hartge EU, Poggioda M, Reimers C, Schweir D, Gruhn G, Werther J (2006) Flowsheet simulation of solids processes. KONA 24:146–158
Hendrickson G (2006) Electrostatics and gas-phase fluidized-bed polymerization wall sheeting. Chem Eng Sci 61:1041–1064
Ibrehema AS, Hussaina MA, Ghasemb NM (2009) Modified mathematical model for gas-phase olefin polymerization in fluidized-bed catalytic reactor. Chem Eng J 149:353–362
Idol JD (1959) US Patent 2,904,580
Jacob SM, Gross B, Voltz SE, Weekman VW (1976) AIChE J 22:701–713
Jazayeri B (2003) Applications for chemical production and processing. In: Yang W-C (ed) Chapter 16 in handbook of fluidization and fluid-particle systems. Marcel Dekker, New York
Jiang P, Wei F, Fan L-S (2003) General approaches to reactor design. In: Yang W-C (ed) Chapter 12 in handbook of fluidization and fluid-particle systems. Marcel Dekker, New York
Kaarsholm M, Rafii B, Joensen F, Cenni R, Chaouki J, Patience GS (2010) Kinetic modelling of methanol-to-olefin reaction over ZSM-5 in fluid bed. Ind Eng Chem Res 49:29–38
Kaminski W (1998) Highly active metallocene catalysts for olefin polymerization. J Chem Soc Dalton Trans 1413–1418
Karri SBR, Werther J (2003) Gas distributor and plenum design in fluidized beds. In: Chapter 6 in handbook of fluidization and fluid-particle systems. Marcel Dekker, New York
Kiashemshaki A, Mostoufi N, Sotudeh-Gharebagh R (2006) Twi-phase modelling of a gas-phase polyethylene fluidized-bed reactor. Chem Eng Technol 61:3997–4006
Knowlton TM (2003) Cyclone separators. In: Chapter 22 in handbook of fluidization and flui-particle systems. Marcel Dekker, New York
Kunii D, Levenspiel O (1969) Fluidization engineering. Wiley, New York
Kunii D, Levenspiel O (1991) Fluidization engineering, 2nd edn. Butterworth-Heinemann, Boston
Mars P, van Krevelen DW (1954) Chem Eng Sci Suppl 3: 41
McAuley KB, Talbot JP, Harris TJ (1994) A comparison of two-phase and well-mixed models for fluidized bed polyethylene reactors. Chem Eng Sci 49:2035
McAuley KB, Macdonald DA, McLellan PJ (1995) Effects of operating conditions on stability of gas-phase polyethylene reactors. AIChE J 41:868–879
Mills PL, Randall HT, McCracken JS (1999) Redox kinetics of $VOPO_4$ with butane and oxygenusing the TAP reactor system. Chem Eng Sci 54:3709–3722
Minchiner A (2014) Made in China. Chem Engineer 872:42–45
Mostoufi N, Cui H, Chaouki J (2001) A comparison of two- and single-phase models for fluidized-bed reactors. Ind Eng Chem Res 40:5526–5532
Moughrabiah WO, Grace JR, Bi XT (2012) Electrostatics in gas-solid fluidized beds for different particle properties. Chem Eng Sci 75:198–208

Park T-Y, Froment GF (2004) Analysis of fundamental reaction rates in the methanol-to-olefin process on ZSM-5 as a basis for reactor design and operation. Ind Eng Chem Res 43:682–689
Patience GS (1990) Hydrodynamics and reactor modelling. PhD Dissertation, Ecole Polytechnique de Montreal
Patience GS, Bockrath RE (2010) Butane oxidation process development in a circulating fluidized bed. Appl Cat A 376:4–12
Patience GS, Bockrath RE, Sullivan JD, Horowitz HS (2007) Pressure calcination of VPO catalyst. Ind Eng Chem Res 46:4374–4381
Pitault I, Nevicato D, Forrissier M, Bernaed J-R (1994) Kinetic model besed on a molecular description for catalytic cracking of vacuum gas oil. Chem Eng Sci 49:4249–4262
Puettemann A, Hartge EU, Werther J (2012a) Application of flowsheet simulation concept to fluidized-bed reactor modelling. Part I: development of a fluidized-bed reactor model. Chem Eng Proc 60:86–95
Puettemann A, Hartge EU, Werther J (2012b) Application of flowsheet simulation concept to fluidized-bed reactor modelling. Part II: application to the selective oxidation of n-butane to maleic anhydride in a riser/regenerator system. Chem Eng Proc 57–58:86–95
Pugsley T, Patience GS, Berruti F, Chaouki J (1992) Modelling the catalytic oxidation of n-butane to maleic anhydride in a circulating fluidized-bed reactor. Ind Eng Chem Res 31:2652–2660
Riazi MR (2005) Characterization and properties of petroleum frsctions. ASTM, Conshohocken, PA
Roy S, Dudukovic MP, Mills PL (2000) A two-phase compartment model of the selective oxidation of n-butane in a circulating fluidized-bed reactor. Catal Today 61:73–85
Sadeghbeigi R (2012) Fluid catalytic cracking handbook, 3rd edn. Elsevier, New York
Sax NI (1975) Dangerous properties of industrial materials. Van Nostrand Reinhold, New York
Secchi AR, Neumann GA, Gambetta R (2013) Gas fluidized bed polymerization. In: Passos ML, Barrozo MAS, Mujumdar AS (eds) Chapter 2 in fluidization engineering: practice. Laval, Canada
Shamiri A, Hussain MA, Mjalli FS, Mostoufi N (2011) Dynamic modelling of gas-phase propylene homopolymerization in fluidized-bed reactors. Chem Eng Sci 66:1189–1199
Sookai S, Langanhoven PL, Shingles T (2001) Scale-up and commercial reactor fluidization-related experience with Synthol gas-to-liquid fuel dense phase fluidized-bed reactors. In: Fluidization X. United Engineering Foundation, New York, pp 621–626
Thompson LM, Bi H, Grace JR (1999) A generalised bubbling turbulent fluidized-bed reactor model. Chem Eng Sci 54:2175–2185
Van Ness K, Van Westen HA (1951) Aspects of the constitution of mineral oils. Elsevier, New York
Venuto PB, Habib TE (1979) Fluid catalytic cracking with zeolite catalysts. Marcel Dekker, New York
Vollert J, Werther J (1994) Mass transfer and reaction behaviour of a circulating fluidized-bed reactor. Chem Eng Technol 17:201–209
Voltz SE, Nace DM, Weekman VW (1971) Application of a kinetic model for catalytic cracking. Ind Eng Chem Proc Des Dev 10(4):530–541
Weekman VW (1968) A model for fluidized catalytic cracking. Ind Eng Chem Proc Des Dev 7:90
Wong R, Pugsley T, Berruti F (1992) Modelling the axial voidage profile and flow structure in the riser of a circulating fluidized bed. Chem Eng Sci 47:2301–2306
Xie T, McAuley KB, Hsu CC, Bacon DW (1994) Gas-phase ethylene polymerization: production processes, polymer properties and reactor modelling. Ind Eng Chem Res 33:449–479
Yamamoto R, Uetake S, Ohtani Y, Kikuchi Y, Doi K (1998) US Patent 5,753,191
Yates JG (1983) Fundamentals of fluidized-bed chemical processes. Butterworths, London
Zhou H, Wang Y, Wei F, Wang D, Wang Z (2008) Kinetics of the reactions of the light alkenes over SAPO-34. Appl Catal 348:135–141